ISSN 0915-633X

NATIONAL INSTITUTE FOR FUSION SCIENCE

Molecular Dynamics of Strongly-Coupled Multichain Coulomb Polymers in Pure and Salt Aqueous Solutions

M. Tanaka, A. Yu Grosberg and T. Tanaka

(Received - Nov. 6, 1998)

NIFS-579 Nov. 1998

RESEARCH REPORT
NIFS Series

NAGOYA, JAPAN

Molecular Dynamics of Strongly-Coupled Multichain Coulomb Polymers in Pure and Salt Aqueous Solutions

Motohiko Tanaka[1], A.Yu Grosberg[2,3], and Toyoichi Tanaka[2]

[1] *National Institute for Fusion Science, Oroshi-cho, Toki 509-5292, Japan*
[2] *Massachusetts Institute of Technology, Cambridge, Massachusetts 02139, USA*
[3] *Institute of Biochemical Physics, Russian Academy Sci., Moscow 117977, Russia*

Abstract

The multichain effect and also the effect of added salt on randomly co-polymerized charged polymers (polyampholytes) in a Langevin fluid are studied with the use of molecular dynamics simulations. The monomers of opposite signs tend to form loose complexes, which makes the Coulomb force attractive on average. With multichain polyampholytes, the typical state at high temperature is a container-bound one-phase state of separated chains with a substantial void among them. The association and dissociation processes occur repeatedly, with the former process a few times faster than the latter. A glass transition occurs when temperature is lowered. A compact and glassy globule in a segregated phase, which resembles that of a single-chain polyampholyte, is a typical state at low temperature due to the Coulomb force. The probability of losing that state is as low as $P_{dis} \sim \exp(-N^{3/2})$, with N the number of monomers. The critical temperature defined by overlapping of the chains increases with molecular weight and stiffness of the chains, and is less sensitive to the number of the chains. An alternate charge sequence makes a difference only when its block size is quite small. The addition of salt suppresses the formation of a dense globule by shielding the electric field; however, this is not effective when the salt ions are not allowed to penetrate well into the globule.

Keywords: molecular dynamics, polyampholyte, multichain, strongly-coupled system, glass transition, salt electrolyte solution.
PACS Numbers: 36.20.Ey, 52.25.Wz, 61.25.Hq, 82.35.+t, 64.60.Cn.

I. INTRODUCTION

Electrically charged polymers are interesting research objects in physics and chemistry. They combine the nature of a strongly-coupled Coulomb system at room temperature due to microscopic scales on the Angstrom range with the peculiarities of the chain-like molecular structure. These polymers have a wide variety of industrial applications due to liquid-like plasticity and good solubility with respect to pure water and salt aqueous solutions[1]. In daily life, charged polymers are often encountered in the form of gels. In biological organisms they are also numerous, including proteins[2] and as nucleic acids of DNA and RNA.

Charged polymers are classified into two large groups, called *polyelectrolytes* and *polyampholytes*. The former type of polymer has a backbone that consists of monomers of one charge sign (apart from interleaving neutral monomers). This type, which is usually accompanied in solution by neutralizing counter-ions[3], is widely utilized as industrial materials. DNA and RNA molecules in the living cells are also of that type. Polyampholytes, on the other hand, are the polymers that are composed of both positively and negatively charged monomers[4]. Importantly, polyampholytes are *heteropolymers*, and the combination of attraction and repulsion long range Coulomb forces creates multiple frustrations[5]. Obviously, properties of polyampholytes depend on overall *composition*, i.e. how many positively and negatively charged monomers are there in the chain. As with other heteropolymers, more delicate properties are determined by the specific *sequence* in which positive and negative monomers are connected one after another in the chain. Furthermore, this sequence may be *annealed* or *quenched* depending on the pK (ionization potential) of the monomers involved and on the pH in solution. An early study of polyampholytes concerned mostly with the annealed ones, in analogy with proteins whose ionic characteristics depend on pH due to the presence of both acidic and basic components[4]. Recent studies have mostly related to the quenched polyampholytes whose characteristics are independent of pH since their charge sequences are predetermined by synthesis chemistry. In a series of experimental works[4,6,7], special emphasis was placed on the conformation and solubility of polyampholytes with respect to water and salt aqueous solutions.

Recent experimental activity in the field of polyampholytes was accompanied by the series of theoretical works. It was pointed out in the work[8] that the Debye-Hükkel attraction effect between charge density fluctuations should exist and lead to compaction of typical quenched polyampholytes. This effect appears unusually sensitive to the overall charge of the chain, as it was shown first by Kantor and Kardar[9]. Specifically, spherical globule is formed when chain is neutral, but it becomes elongated, or even adopts the necklace shape, when charge offset becomes of order or greater than $\sqrt{N}$, N being the number of charged monomers. The most complete work in this direction[10] investigated shape and stability of polyampholyte globule in terms of a simple Flory theory. Recently, the multichain effect and the phase equilibrium in pure water and salt-added solution were examined[11], and the single-chain theory was shown to apply only to an exponentially dilute solution of polyampholytes. Obviously, all the works deal with those properties of polyampholytes which are composition-dependent, but sequence insensitive. An attempt to look into sequence specific properties was undertaken in the work by Pande et al.[12].

Numerically, singlechain polyampholytes were first studied by a Monte Carlo simulation with the use of the lattice model[9], and a few years later by a molecular dynamics (MD) simulation of the non-lattice

type[13]. In the former, the effects of unbalanced charge and temperature were examined and found to be in reasonable agreement with the single-chain theory. The latter study, which examined the dynamical process and equilibrium properties, was the first to show the existence of a dense globular state at low temperature under the non-lattice model. It also demonstrated a hysteresis that the volume (i.e., the gyration radius) of the polyampholyte undergoes when the temperature changes slowly. This is the result of cooperation between the Coulomb and short-range attraction forces. The effect of an applied electric field on the stretching properties of polyampholytes was studied quite recently with a MD simulation[14] (note that this effect is sequence specific).

Owing to these experimental and theoretical studies, our understanding of polyampholytes has greatly advanced. From a numerical point of view, it is worthwhile extending the research from single-chain to multichain cases in order to know precisely how the results for the single-chain polyampholytes are related to the case of multichain polyampholytes[11], which is the usual case for experiments with aqueous solutions. Specifically, we are interested in the dynamics of chain association and dissociation, stability of collapsed complexes, and occurrence of glass transition. Other interesting points are to quantify the precise effect of charge sequence, molecular weight, and that of added salt on the properties of the polyampholytes. The present paper is devoted to numerical studies of these issues of isolated (container bound) polyampholytes by means of molecular dynamics simulations. Further study of multichain polyampholytes in the periodic system is described in a separate paper[15] with the use of the Ewald sum method[16,17].

In this study, we adopt model polyampholytes that are comprised of various numbers of equal length chains, each of which contains between 16 and 64 charged monomers. These are the randomly copolymerized polyampholytes, whose charge sequences are randomized across the chains by shuffling the already charge-assigned monomers. We impose the condition that the sum of all the charges of the polyampholyte is null. (Counter-ions are not introduced, except for salt ions in Sec. IV.) In addition to the polyampholytes made of random co-polymerization, we also performed a series of runs with alternate sequences in order to delineate the influence of the sequences. These results are described in Sec. III.

II. THE EQUATIONS OF MOTION

In the molecular dynamics simulations of this paper, the position and velocity of the monomers evolve in time following Newton's equations of motion,

$$m\frac{d\mathbf{v}_i}{dt} = \mathbf{F}_{LR}(\mathbf{r}_i) - \frac{3T}{a^2}(2\mathbf{r}_i - \mathbf{r}_{i+1} - \mathbf{r}_{i-1}) + \mathbf{F}_{th} - \nu m\mathbf{v}_i, \quad (1)$$

$$\frac{d\mathbf{r}_i}{dt} = \mathbf{v}_i. \quad (2)$$

Here, $\mathbf{r}_i$ and $\mathbf{v}_i$ are the position and velocity of the i-th monomer ($i = 1 \sim N$), respectively, m is the monomer mass, T the temperature, a the normalization length (which is close in value to the bond length of the monomer pairs), and ν the friction constant. The Coulomb force $\mathbf{F}_{LR}$, which is an electrostatic long-range force, is obtained by summing over all the possible monomer pairs,

$$\mathbf{F}_{LR}(\mathbf{r}_i) = \sum_j \frac{Z_i Z_j e^2}{\epsilon\,|\mathbf{r}_i - \mathbf{r}_j|^2}\hat{\mathbf{r}}_{ij}, \quad (3)$$

where Z_i is a charge state ($Z_i = \pm 1$), ϵ the electrical permitivity, and $\hat{\mathbf{r}}_{ij}$ a unit vector along the line $(\mathbf{r}_i - \mathbf{r}_j)$. In eq.(1), a harmonic spring force of entropic nature is adopted to account for the connection of two adjacent monomers. The thermal

force $\mathbf{F}_{th}$ that exerts random kicks on the monomers is generated with the use of random numbers with a Gaussian distribution in each time step. The strength of the thermal kicks is controlled in such a way that the average kinetic energy of the monomer equals $\frac{3}{2}k_BT$ in balance with the momentum absorption by the immobile solvent[13]. (Energy units are hereafter used in which the temperature T stands for k_BT, with k_B the Boltzmann constant.)

The set of equations, Eqs.(1)-(3), explicitly involves two non-dimensional parameters. These are the electrostatic coupling constant $\Gamma = e^2/\epsilon aT$ and the friction constant ν/ω_p, where $\omega_p = (4\pi n_0 e^2/\epsilon m)^{1/2}$ is the plasma frequency with $n_0 \sim a^{-3}$ an average (positive) charge density. For the CH_2 monomer in pure water and at room temperature, i.e., $\epsilon \sim 80$ and $a \sim 1$ Å, the Coulomb energy prevails over thermal energy, $\Gamma \sim 7$, and $\omega_p \sim 1 \times 10^9 \mathrm{s}^{-1}$. Each monomer has a rigid sphere that the other monomer cannot penetrate into; it is elastically reflected upon entering the distance called the exclusion radius a_{col}. Other parameters that control the properties of polyampholytes are the charge sequences, the molecular weight, and the number of chains that comprise the polyampholytes. These parameters are systematically changed in the simulation runs in Sec. III and Sec. IV. The standard parameters $a_{col} = 0.5a$ and $\nu = 0.03\omega_p$ are used unless otherwise specified.

In the following sections, we deal with the multichain polyampholytes that are confined within a spherical shell of radius $R = 21a$, which is filled with a Langevin fluid. (Refer to Ref.15 for multichain polyampholytes in the periodic system.) The monomers hitting the boundary surface are reflected elastically, but the electric field is not distorted there. Except for the alternate sequences in Sec. III, the polyampholytes used in the following sections consist of randomly co-polymerized quenched chains of six 32-mers, with the constraint of overall charge neutrality. Thus, an individual chain is not neutral, having typically a charge of order $\pm e\sqrt{N_1}$, where N_1 is the number of monomers on a chain.

III. MULTICHAIN POLYAMPHOLYTES IN PURE SOLVENTS

A. Time evolution of multichain polyampholytes

A typical time evolution of a multichain polyampholyte is shown by the bird's-eye view snapshots of Fig. 1. Here, the polyampholyte is composed of eight flexible chains of 32-mers with an exclusion radius of $a_{col} = 0.5a$. The temperature is $T/T_0 = 1/2$, where T_0 is the base temperature for which the coupling constant becomes unity, i.e., $\Gamma_0 = e^2/\epsilon a T_0 = 1$. The initial configuration of a small droplet expands to the separated chains in Fig. 1(b) after a time $\tau_{eq} \sim 200\omega_p^{-1}$. There is a large void among the chains. The relative positions of the chains continue to fluctuate due to random thermal kicks in the Langevin fluid. Some of the chains remain entangled for a period of time and then are separated for another period of time, as seen in Figs. 1(b) and (c). The above relaxation time corresponds to $\tau_{eq} \sim 2 \times 10^{-7}$sec for the CH_2 monomer in pure water ($\epsilon = 80$).

Figure 2 shows the time history of several quantities for the run depicted in Fig.1. The average spring energy per monomer, $W_{spr} = (3T/2a^2) < (\Delta r^{(c)})^2 >$, in the top-left panel adjusts itself and levels off to the equilibrium value $\frac{3}{2}T$, which equals the average kinetic energy. This manifests equi-partition of the oscillation energy. The middle-left panel shows the Coulomb energy per monomer, Φ_{ES}, normalized by the base thermal energy T_0, defined as

$$\Phi_{ES} = \frac{1}{N}\sum_i \sum_{j>i} \frac{Z_i Z_j e^2}{\epsilon\,|\mathbf{r}_i - \mathbf{r}_j|}, \qquad (4)$$

A large change in the Coulomb energy

takes place in the initial transient stage because local charge rearrangement occurs for which the deviation $\Delta\Phi_{ES} \sim e^2/\epsilon r_{ij}$ is relatively large. Subsequent changes are due to the global relaxation of the conformations, which are inversely proportional to the size of the polyampholyte and small in magnitude. The bond length between the connected monomers $\Delta r^{(c)}$ remains almost constant although they are loosely connected by harmonic springs.

The top-right panel depicts the *system* gyration radius $R_{g,sys}$ that includes all the monomers of the polyampholyte, and the middle-right panel shows the average gyration radius of the chains R_{g1}. These radii are defined, respectively, as

$$R_{g,sys} = \left(\frac{1}{N} \sum_{j=1}^{N} (\mathbf{r}_j - < \mathbf{r} >)^2 \right)^{1/2}, \quad (5)$$

$$R_{g1} = \frac{1}{N_c} \sum_{s=1}^{N_c} \left(\frac{1}{N_1} \sum_{j=1}^{N_1} (\mathbf{r}_j - < \mathbf{r}_s >)^2 \right)^{1/2} \quad (6)$$

where N is the number of all the monomers, and N_c is the number of chains, i.e., $N = 192$, $N_c = 6$, and $N_1 = 32$. As earlier noted, each chain has a small net charge under random co-polymerization. The system gyration radius increases to $R_{g,sys} \sim 12a$ on the time scale $\tau_{eq} \sim 200\omega_p^{-1}$, which is the value allowed for a system whose radius is limited to $R = 21a$. The diffusion speed of the chains can be deduced by $V_{dif} = dR_{g,sys}/dt$. It becomes $\sim 0.12a\omega_p$ in the early time $\omega_p t < 50$, which is about one third that of the thermal speed $v_{th} = (3/4\pi\Gamma)^{1/2}$ ($\Gamma = T_0/T$). Except for this early phase, the diffusion speed is $V_{dif} \sim 0.02a\omega_p$ on average , which is about 5% that of the thermal speed.

As stated above, the slow changes in the Coulomb energy and the system gyration radius occur simultaneously. On the other hand, the average gyration radius of the chains oscillates around the value $R_{g1} \sim 4a$. The velocity V_x of an individual monomer exhibits amplitude oscillations whose period is longer than the friction time ν^{-1}. This should correspond to large structure fluctuations of the polyampholyte, since fast oscillations without energy sustainment are damped and wiped out in a Langevin fluid.

The temperature variation of the typical relaxed conformations of the multichain polyampholyte is shown in Fig. 3 for three temperatures: (a) $T/T_0 = 1$, (b) $T/T_0 = 1/4$, and (c) $T/T_0 = 1/8$. All the plots are drawn on the same scale, with the size of the negative monomers (dots, $a_{col} = 0.5a$) prorated. At high temperature, i.e., case (a), the polyampholyte is made up of elongated coils whose mass centers distribute homogeneously in the finite domain. As the temperature is lowered to that of case (b), there occurs a change from a one-phase state with scattered coils to a segregated phase with globules; their life in pairs is still short and mostly they live separately. When the temperature is further lowered as in case (c), the chains form a compact globule that cannot be distinguished from the one consisting of a single continuous chain. Note that the globule keeps a spherical shape having a nearly fixed radius and a distinct edge, with not a single monomer straying outside. As will be mentioned later, the monomers in a compact globule of Fig. 3(c) continue to vibrate under thermal agitations from surrounding medium. These evidences indicate that the compact globule is in the *glass* state, which is virtually a natural state of the low temperature polyampholyte[8], irrespective of the boundary conditions of the domain.

We note here that freezing is much easier to achieve on the lattice than in any off lattice systems. The final state of the folding process with the use of the lattice model (of a small size) appears to be well defined due to such quantization that the energy gap between adjacent levels near the energy minimum is set a little too large to allow

for thermal fluctuations. In this regard, off-lattice models like molecular dynamic simulations have obvious advantages compared to lattice models to study a thermally fluctuating state adopted by the chains. On the other hand, the very concept of freezing needs careful formulation and definition for any off-lattice systems.

B. Statistical properties of multichain polyampholytes

Figure 4 highlights the effect of the Coulomb force by displaying side by side the results for charged and non-charged polymers. Each data point in the figure (and also in the following figures with the same format, viz., Figs. 5, 6, 7, 8, 11 and 12) is an average over twenty independent runs with polyampholytes of different charge sequences (random but overall charge neutrality) and initial conformations. In panels (a) and (b) of Fig. 4, the system and average gyration radii are shown, respectively, as functions of temperature. Here, the polymers are comprised of six 32-mers. For the non-charged polymers, neither of the two gyration radii $R_{g,sys}$ or R_{g1} depends on temperature. Insensitivity of the gyration radius of each chain on temperature is expected for the entropic elasticity adopted in Eq. (1). The charged polymers here are quenched polyampholytes of random co-polymerization, for which deviations from the non-charged polymers are evident in the low temperature regime $T/T_0 < 1$ where the Coulomb energy much exceeds the thermal energy. On the other hand, differences are small at high temperature. The figure clearly shows that the Coulomb force is attractive on average for randomly co-polymerized polyampholytes. (Qualitatively similar results are found also in the periodic system[15].)

Figure 4(c) depicts *the filling index* that indicates the degree of chain overlapping or entanglement, defined as

$$\zeta \equiv N_c^{1/3} R_{g1}/R_{g,sys}. \qquad (7)$$

The criterion that the polyampholyte resides in a segregated phase and is non-soluble with respect to the solvent is given by the condition $\zeta \geq 1$. This corresponds to close overlapping of the chains and the network formation. In the opposite condition, $\zeta < 1$, the polyampholyte is considered to be transparent for the light scattering experiments and soluble to the solvent. The filling index for the polyampholyte in Fig. 4(c) is larger than unity at low temperature. The critical temperature defined by the condition $\zeta = 1$ is $T_*/T_0 \sim 0.17$ for the standard parameters. This coincides with the observed temperature at which the one-phase state (separated chains) replaces the segregated phase (globule) in the molecular dynamics simulations. On the other hand, the non-charged polymers are soluble for the entire temperature range shown in the figure. These features are consistent with the theory of multichain polyampholytes[11].

The attractive nature of the Coulomb force for polyampholytes is also found in Table I. At low temperature $T/T_0 \leq 1/4$, the possibility of opposite-sign charges being the nearest monomer pairs (not necessarily the connected monomer pairs) is significantly larger than that of equal-sign charges. Also, the distance between monomers of opposite-sign charges is smaller than that with equal-sign charges, which implies the formation of loose complexes of positive and negative monomers. At high temperature $T/T_0 = 1$, the difference between the charge pairs is small, which is consistent with the similarity of charged and non-charged polymers at a similar temperature shown in Fig. 4. When we look at a sphere of radius $1.5a$ centered on a monomer, the average number of surrounding monomers having different sign charges is always larger than that with equal-sign charges, as shown in the bottom part of Table I.

Figure 5 shows the effect of chain stiffness on the size of polyampholytes. The

size of a flexible polyampholyte is always larger than that of a stiff one at a given temperature, except at high temperature where the system gyration radius approaches the limit set by the domain size. The system gyration radius is an increasing function of temperature: $R_{g,sys} \propto T^{0.7}$ for flexible chains, and $R_{g,sys} \propto T^{1.1}$ for stiff chains. These dependences for multichain polyampholytes are more sensitive than the scaling $R_g \propto T^{1/3}$ for single-chain polyampholytes[13], which is attributed to the growth of a large void space among the chains.

As the multichain effect of polyampholytes appears more strongly in their global size, the filling index for the stiff chains becomes larger than that for the flexible chains. The critical temperature for chain overlapping to occur shifts from $T_*/T_0 \sim 0.17$ for the flexible chains to $T_*/T_0 \sim 0.33$ for the stiff chains.

The Coulomb energy per monomer defined by Eq. (4) is depicted in Fig. 6(a) as a function of temperature. By comparison of Figs. 5 and 6, the Coulomb energy is found to be inversely proportional to the gyration radius of each chain, $\Phi_{ES} \propto R_{g1}^{-1}$. This is quite understandable since the major contribution to the Coulomb energy arises from the adjacent monomer pairs whose distance is almost proportional to the gyration radius R_{g1} in the one-phase state. The contribution of the global conformation to Φ_{ES} is small, but is nevertheless decisive for the large-scale structure formation.

Very interestingly, the slope of the curve of the Coulomb energy in Fig. 6(a) changes suddenly at $T/T_0 \sim 0.2$. This leads to a jump in the heat capacity $C_{coul} = \partial\Phi_{ES}/\partial T$ at that temperature, indicating occurrence of a phase transition of the internal structure of multichain polyampholytes. This transition occurs at a temperature where the morphological change between the one-phase state and the segregated phase takes place.

The phase transition is also identified in Fig. 6(b), which shows the time deviation of the monomer distance:

$$\Delta_{ij} = \frac{2}{N(N-1)} \sum_i \sum_{j>i} \delta r_{ij} / < r_{ij} > . \tag{8}$$

Here, δr_{ij} is the time deviation of the monomer distance r_{ij} between the i-th and j-th monomers. The summation is made over all possible pairs of the N monomer system. For the flexible chains, the ratio is nearly constant for the two entry points in the segregated phase at $T/T_0 < 0.2$. Then, the ratio decreases as the temperature increases; it hits the bottom and begins to increase at $T/T_0 \sim 0.35$, since the deviation of the distance δr_{ij} continues to increase with increasing temperature while an increase in the average distance $< r_{ij} >$ is suppressed by the wall at high temperature. The transition at $T/T_0 \sim 0.2$ marks the crossover of the glass phase and the neutral phase, where the Coulomb interaction dominates over the thermal fluctuations in the glass phase. For stiff chains, everything shifts to the higher temperature side.

C. The effect of alternate sequences

It is predicted that a polyampholyte comprised of chains of alternate sequences has less of a tendency to make neutral complexes, and thus is more easily soluble in water[11]. To examine such effects with alternate sequences, a series of molecular dynamics simulations are performed, in which each of the six 32-mer chains is composed of alternating blocks of positively and negatively charged monomers. The length of the block (the number of monomers in a block) is taken to be one, two, and then four.

Figure 7 shows that polyampholytes with complete alternating sequence with a block length of unity $(+ - + - ...)$ have a larger system gyration radius than those with a block length two and four in the Coulomb phase, for which $T/T_0 < 0.2$ for the flexible

polyampholytes ($a_{col} = 0.5a$). For chains with large block lengths, we find complexes of positive and negative blocks. The gyration radius for the alternate sequence of block length four is already close to that for the randomly co-polymerized sequence described in Sec. III(b).

The gyration radius of each chain R_{g1} in Fig. 7(b) depends on the sequence, which is reduced as the block size of one charge-sign becomes large in the Coulomb phase. The filling index $\zeta = N_c^{1/3} R_{g1}/R_{g,sys}$ in Fig. 7(c) decreases as the block length increases from one to four. Quite remarkably, in terms of the filling index, a polyampholyte with alternate sequence of block length four behaves just like one synthesized by random co-polymerization. Thus, the charge sequence significantly affects polyampholyte properties only if it is completely alternate.

D. The effect of finite /infinite domains

The diffusion of polyampholyte chains at high temperature is blocked if a boundary wall exists in the computational domain. This is a usual situation for polyampholytes in a solution. On the other hand, it is physically an interesting question whether the globular state at low temperature requires a closed domain of finite volume.

Figure 8 compares runs with finite and infinite domains. The polyampholytes here are again composed of six 32-mers of random co-polymerization (overall charge neutrality), and each data point is obtained by averaging twenty independent runs with different random sequences and initial conformations. For polyampholytes in an infinite volume (filled circles), the upper two data points in Fig. 8(a) keep on growing with time. However, the lower two points residing at $T/T_0 \leq 1/8$ remain there, stationary in time. Moreover, these points superimpose quite well on the open circles in the finite volume.

These results are not strange, since the globule obtained in the low temperature regime has a distinct edge without any monomers straying outside of the globule, irrespectively of the boundary condition of the domain. This point is further confirmed by special long runs that continue up to thirty relaxation times, $15000\omega_p^{-1}$, of the six 32-mer polyampholyte chains. The time history of the system gyration radius is shown in Fig. 9 for the temperatures (a) $T/T_0 = 1/2$, (b) $T/T_0 = 1/4$, and (c) $T/T_0 = 1/8$. The domain is limited by a spherical wall of radius $R = 21a$ except for the run in Fig. 9(d), which run has $T/T_0 = 1/8$. Initial conformations of highly stretched threads of randomly co-polymerized chains with overall charge neutrality are purposely chosen, to avoid artificial trapping of the conformations in a small volume.

The conformations for the medium temperatures, $T/T_0 = 1/2$ and $1/4$, shown in Figs. 9(a) and (b), are the wall-stabilized ones in which the monomers are reflected inward by the elastic wall. Without the wall, infinite diffusion of monomers takes place, and a bound state is not obtained for these temperatures. We see repetition of the dissociation and association processes of the chains, starting at $t \sim 2500\omega_p^{-1}$ and $10000\omega_p^{-1}$ in Fig. 9(b). The molecular dynamics simulation tells us that the association process is about twice as fast as the dissociation process for the medium temperature $T/T_0 \geq 1/4$.

We also notice, by comparing Figs. 9(c) and 9(d), that both of the system gyration radii for the closed and open systems at low temperature $T/T_0 = 1/8$ remain small, and are not much affected by the presence of the boundary wall. There, the polyampholytes form dense globules which remain stationary for times $t > 500\omega_p^{-1}$. The compact globule, which has the characteristics of glass, is thus regarded as a natural state of a low temperature polyampholyte.

The attractive nature of the Coulomb interactions is again verified by the special

run in Fig. 10, where the monomer charges of a randomly co-polymerized polyampholyte (six 32-mers) are suddenly reset to zero at time $t = 4500\omega_p^{-1}$. The time history of the system gyration radius in the top frame shows that the globule that has remained stationary is quickly destroyed, since the chains are no longer under the influence of the Coulomb force. Otherwise, the globule remains as shown in Fig. 9(c). The scatter plots of Fig. 10 labeled (a) and (b) depict, respectively, the conformation with the Coulomb force inclusive and that after the Coulomb force has been switched off. It is interesting that the Coulomb force is strong enough to put the polyampholyte chains together at low temperature, without aid of the boundary wall. However, chain entanglement without actual bonds is unable to prevent the globule from being destroyed.

The stationary globular state at low temperature is thought to arise from enhanced stability by charge pairing, as found in Table I. An increase in temperature removes the pairing, and the globular state is lost by thermal agitation. The above process may be theoretically treated in the following manner. If we treat the chains to lowest order as an assembly of charged particles without internal structures, then the essential part of the free energy may be approximated by adding the Coulomb energy to the free energy of the ideal gas[18],

$$F = NT\log\left(\frac{N/V}{n_Q} - 1\right) + U_{coul}, \quad (9)$$
$$U_{coul} = -A/\epsilon R \sim -A/\epsilon V^{1/3}.$$

Here, the coefficient is positive, $A \sim (e^2 N_1)N_c = e^2 N > 0$, due to the attractive nature of the Coulomb force among the chains. (Inclusion of the chain free energy is desirable in Eq.(9), but free energy maximum occurring at finite volume may not be much affected since F becomes negative infinite both at $V = 0$ and $V = \infty$.) Notably, the free energy given by Eq. (9) possesses a maximum at an intermediate radius R. If we differentiate the free energy in terms of the radius R and equate it to zero, we get

$$R_0(T) = [V_0(T)]^{1/3} = A/\epsilon NT \sim a\Gamma \quad (\Gamma = T_0/T). \quad (10)$$

This reveals that the initial conformation starting with a small radius compared to $R_0(T)$, or the chains initially located within that distance, collapse to a natural state whose radius is less than the radius R_0. This corresponds to the compact globule at low temperature. Moreover, the radius of bifurcation $R = R_0(T) \sim a(T_0/T)$ increases when the temperature is reduced, which makes it possible for more initial conformations and chains to reside in the globule regime. All of these points, including the value of R_0, are in good agreement with the molecular dynamics simulation results.

Finally, we show that the probability for the polyampholyte chains to escape from the compact globule is virtually eliminated at low temperature. For low temperatures $T/T_0 \leq 0.1$, the inter-monomer distance, especially that of the positive and negative pairs, becomes very small, as shown in Table I. The Coulomb energy is dominated by the attractive part. Then, the leading term of the energy gap between the globular state and the one-phase state of scattered coils is given by

$$\Delta E = e^2 N/\epsilon\lambda_D \sim e^3 N^{3/2}/T^{1/2}R^{3/2}, \quad (11)$$

where the Debye length is $\lambda_D = (\epsilon T/4\pi n_0 e^2)^{1/2}$ and $R^3 n_0 \cong N$. Then, the probability for the globule to be destroyed by random thermal agitation is given by

$$P_{dis} = \exp(-\Delta E/T) \sim \exp\left(-e^3 N^{3/2}/\epsilon T^{3/2}R^{3/2}\right) \cong \exp[-(a\Gamma/R)^{3/2}N^{3/2}]. \quad (12)$$

Here, the electrostatic coupling constant $\Gamma = (T/T_0)^{-1}$ varies inversely with the temperature T. An important thing in Eq. (12)

is its scaling with respect to the number of monomers N. For the typical parameters of a low temperature globule, $\Gamma = 8$ and $R/a \sim 3$, the argument of the exponential function becomes $4.4N^{3/2}$. Thus, any reasonable number of monomers for the chains to be regarded as a polymer yields a probability that is extremely small:

$$P_{dis} \propto \exp(-N^{3/2}) <<< 1. \quad (13)$$

This means that once a compact globule is formed at low temperature, it will fall apart only after an astronomically long period of time.

E. Dependence on molecular weight

Figure 11 shows the effect of the length (molecular weight M_w) of the chains on the size of multichain polyampholytes made by random co-polymerization with overall charge neutrality. In the medium temperature regime, the system gyration radius becomes larger for smaller molecular weight, scaling roughly as $R_{g,sys} \sim M_w^{-1/2}$. The gyration radius of each chain R_{g1} behaves like that of a single-chain polyampholyte[13]. At high temperature, it scales as $R_{g1} \sim M_w^{1/2}$, although the radius is only a fraction of that of the Gaussian coil. The filling index in Fig. 11(c) shifts upward with increase in the molecular weight of the chains. The critical temperature that separates the one-phase state and the segregated phase is $T_*/T_0 \sim 0.082$, 0.17, and 0.35 for the chains with 16, 32, and 64-mers, respectively. This is well fitted by the power law, $T_*/T_0 \sim M_w^{1.04}$. Therefore, the polyampholyte consisting of longer chains becomes more difficult to dissolve in neutral solvents.

On the other hand, the dependence on the number of chains is less remarkable in Fig. 12. When the number (192) of monomers is fixed, which has the effect of maintaining the Coulomb interaction at the same level, the system gyration radius of an eight-chain polyampholyte is slightly larger than that of a four-chain polyampholyte in the temperature range of $0.1 < T/T_0 < 1$. This is rather straightforward, since a larger number of chains means more freedom for the conformational organization. Accordingly, the filling index decreases as the number of chains increases in the above temperature range.

However, the dependence on the number of chains becomes almost invisible when the molecular weight of each chain is kept the same. In this case, the freedom for expansion due to the increase in the number of the chains may be compensated by an intensified Coulomb force that compresses the polyampholyte.

F. Oscillations in multichain polyampholytes

When we take a precise look at the motion of each chain, we find slow oscillations in the gyration radius and the velocity of the monomers. We note in passing that the eigen oscillations are suppressed by the friction of a Langevin fluid. The slow oscillations should correspond to transformation of the conformation between elongated coils and a loose globule; this is inferred by comparison of the snapshots (b) and (c) of Fig. 1 (the oscillatory motions are clearly seen in a video movie). A spectral analysis of the time series data of the gyration radius R_{g1} was made with the use of the maximum entropy method[19]. The maximum entropy method is very powerful for spectral analysis of non-stationary quantities under growth or attenuation. (The spectral peaks are obtained with high accuracy, but the height of the peaks does not correspond to the power spectral density.) Figure 13 shows that each chain undergoes slow oscillations. At high temperature, we see oscillations in most of the chains that are separated from each other. The period of oscillations has a range in value: $\tau \sim 60 - 100\omega_p^{-1}$. At low temperature, the chains lump up as a globule, and only a small number of chains make oscillations

whose period is longer than that at high temperature.

The velocity of the sampled monomers also oscillates. At high temperature, the frequency band is broad, extending over $\tau = 6 - 60\omega_p^{-1}$. Only the low frequency part ($\omega < 2\pi\nu$) is related to changes in the global conformation. At low temperature, the oscillations are limited to a narrow band whose period is $\tau \sim 30 - 60\omega_p^{-1}$, implying less freedom for conformational changes.

IV. POLYAMPHOLYTES IN SALT AQUEOUS SOLUTION

Addition of salt to a solution with precipitated polyampholytes is expected to screen the internal electric field among the monomers, and to loosen the binding of the monomers within the globules, which causes dissolution of the polyampholyte[8]. Such effects of salt may be studied by placing free counter-ions in the multichain polyampholyte system. In the following run, the polyampholyte consists of six 32-mers of random co-polymerization with overall charge neutrality. The initial positions of the chains are sufficiently separated such that the mass-centers of the six chains are placed at $\pm 3.5a$ on the x, y, and z-axis. We introduce the same number of positive and negative counter-ions, with their mass and charge equal to those of the chained monomers. The reflecting wall is placed at radius $R = 17.5a$ for the polyampholyte, whereas the wall is set at $R = 14a$ for the counter-ions for the purpose of computational efficiency. This treatment is justified since the polyampholyte is confined in the latter volume at low temperatures where the effect of added salt is most predominant.

Figure 14 shows the effect of salt (512 salt ions, with half positive ions and the other half negative ions). Each data point in this figure is an average over ten independent runs with polyampholytes of different charge sequences and initial conformations. Evidently, the system gyration radius of polyampholytes increases by addition of salt, which affects preferentially the low temperature regime, $T/T_0 \leq 0.3$, for the flexible chains ($a_{col} = 0.5a$). The gyration radius of each chain becomes slightly larger in the presence of salt ions. The critical temperature at which the filling index becomes unity, $N_c^{1/3} R_{g1}/R_{g,sys} = 1$, is $T_*/T_0 \sim 0.17$ in a pure solvent. After addition of salt, the filling index is reduced to less than unity in the entire temperature range shown in Fig. 14(c), which means dissolution of polyampholytes.

The above results indicate that the electric field binding the monomers has been screened by the salt ions. This point is directly proven by the salt-free simulation where the electrical permitivity strength in Eq.(3) is increased to $\epsilon = 2\epsilon_0$, with ϵ_0 the original value in the salt-free solution. The triangles in Fig. 14 depict the case with enhanced electrical permitivity, which nicely reproduce all the results for 512 salt ions.

The density of the polyampholyte localized within the globule is $n_{PA} \sim 0.62a^{-3}$ at $T/T_0 = 1/8$. The salt density due to 512 counter-ions is $n_{sal} \sim 512/(14a)^3 \sim 0.19a^{-3}$. The added salt, whose density is a fraction of that of the polyampholyte, is already as effective as the electrolyte solution with $\epsilon > \epsilon_0$ in its ability to loosen the globule. This density is somewhat less than, but qualitatively in agreement with, the prediction by Higgs and Joanny[8].

The typical relaxed conformation of the polyampholyte in the salt aqueous solution is shown in Fig. 15(a) for $T/T_0 = 1/8$. Fig. 15(b) shows only chained monomers of the polyampholyte in Fig. 15(a). In the presence of salt, a mixture of a loose globule and separated chains is obtained, for which $\zeta < 1$. For comparison, conformation of the polyampholyte in the pure solvent is shown in Fig. 15(c) for the same temperature. This dense globule is in clear contrast

with the loose one in the salt aqueous solution.

Finally, we obtained two simulation results that reveal the subtlety of the effects of salt, especially at low temperature. First, half the number (256) of salt ions, each of which carries twice more amount of charges, have the same effect as the standard salt of basic charge. However, for very low temperatures $T/T_0 \leq 0.1$, half the number of salt ions with double the charges are less effective than the ordinary salt ions, due to less homogeneity of the salt ions. Here appears a discreteness effect in the effectiveness of salt.

Secondly, when the polyampholyte chains are placed in close proximity to each other before salt addition, the size of salt-added polyampholyte increases but very slowly. Figure 16 shows the system gyration radius for the runs in which 512 salt ions are placed at the intermediate time $t = 1300\omega_p^{-1}$ in a region not occupied by the already-formed globule of six 32-mers. For both the temperatures shown in the figure, the globule begins to swell upon addition of salt ions. Some of the chains are eventually separated from the globule, and the system gyration radius approaches the value of the salt-added case shown in Fig. 14. But, the expansion occurs several times slower, $\tau_{gl} \sim 2500\omega_p^{-1}$, than that for the case when the globule is not formed at all, $\tau_{sal} \sim 500\omega_p^{-1}$.

These observations are uniquely explained by the ability of salt ions to penetrate among the polyampholyte chains and globules. Namely, lighter salt ions have easier and more homogeneous access to inside the globules, with more effectiveness when the globules are less tight. The use of the continuous fluid model with enhanced electrical permitivity is thus not very accurate in these cases.

V. SUMMARY AND CONCLUSION

In this paper, the multichain effect and also that of added salt on randomly co-polymerized polyampholytes have been studied. For high temperature, a container-bound one-phase state with homogeneously scattered chains is obtained due to confinement in the finite volume (Fig.1). Polyampholyte expansion occurs in about 5% of the thermal speed on average; the typical expansion time is $\tau \sim 200\omega_p^{-1}$ (Fig.2), which corresponds to the microsecond range for the CH_2 monomers in pure water. The size of a multichain polyampholyte becomes much greater than that of a single-chain polyampholyte at high temperature, due to the growth of a large void space among the chains (Fig.3).

At medium and low temperature, the role of the Coulomb force, which is attractive on average, is predominant; the monomers tend to associate and form loose complexes (Figs.3 and 4). The association and dissociation processes occur repeatedly at medium temperature, where the former process occurs a few times faster than the latter (Fig.9). At very low temperature, a compact globule in the state of glass with a distinct round surface is formed both for the single and multichain polyampholytes. The entanglement of the chains without actual bonds between the chain elements is not enough to sustain the globule; the monomers in the globule diffuse away when the Coulomb force is switched off (Fig.10).

The stationary globular state at low temperature is thought to arise from enhanced stability by charge pairing (Table I). An increase in temperature removes the pairing, and the globular state is lost by thermal agitation. Although the MD simulation time is restrictive to see a real long-time behavior of the polyampholyte chains, an estimate of the lifetime of a collapsed globule by Eqs.(9)-(13) tells that its life is very long, which would be destroyed only after a passage of an astronomical time. The ini-

tial conformations are either on the globule (glass) regime or the coil regime, depending on their volume (cf. Eq.(10)). The probability for the compact globule to be destroyed and transformed to an assembly of scattered chains is estimated to be $P_{dis} = \exp(-\Delta E/k_BT) \sim \exp(-N^{3/2})$ (Eq.(12)), which is infinitesimally small for any realistic value for the number of monomers N. The compact globule is considered to be a natural state in the low temperature regime, irrespective of the boundary condition of the domain (Fig.8).

The size of polyampholytes is affected by the domain size at high temperature where a confining wall (container) limits their diffusion, while it isn't at low temperature (Fig.8). A glass-like compact globule is a natural state of the low temperature regime, as stated above. The results for polyampholytes under the periodic boundary conditions[15] are qualitatively the same as those of isolated (container bound) polyampholytes which were studied in this paper.

The polyampholytes with alternating sequences of positive and negative monomers generally occupy larger volume than do the randomly co-polymerized ones (Fig.7), because the electric field is spatially averaged out. However, such effects are apparent only when the block size of alternating sequences is as small as two. Otherwise, the polyampholytes with alternating sequences behave like randomly co-polymerized polyampholytes.

A good index to measure the denseness of monomers, or the degree of chain entanglement, is the filling index, defined by $\zeta \equiv N_c^{1/3} R_{g1}/R_{g,sys}$, with N_c the number of chains, and R_{g1} and $R_{g,sys}$ the gyration radii of an individual chain and the whole polyampholyte, respectively. The filling index is comparable to or exceeds unity when the chains closely overlap and become entangled. Polyampholytes become more dense when the chain stiffness or the molecular weight of the chains is increased (Figs.5 and 11), whereas they become sparse when the number of chains is increased, though to a lesser degree (Fig.12).

The critical temperature that separates the one-phase state with scattered chains and the segregated phase with a globule is defined by the condition that the filling index becomes unity: $\zeta = 1$. The critical temperature is well fitted by $T_*/T_0 \propto M_w$, with M_w the molecular weight of the chain. A polyampholyte consisting of chains of larger molecular weight is shown to be more difficult to dissolve in salt-free solvents.

Spectral analysis shows slow oscillations of the chains of multichain polyampholytes at high temperature, which corresponds to transformation of the conformation between elongated coils and a loose globule (Fig.13). At low temperature, the oscillation of each chain is not prominent since all the chains are contained in the dense globule. However, the chained monomers are still under thermal vibrations, showing the glass-like nature of the globule (also, Fig.6(b)).

Concerning the effect of added salt, the salt ions diffuse among the monomers of polyampholytes and screen the internal electric field, which loosens and destroys the insoluble globules at low temperature (Fig.15). The salt, whose density reaches a fraction of that of the polyampholyte, behaves like an electrolyte solution that has enhanced electrical permitivity compared to a salt-free solution (Fig.14). This behavior is in agreement with theory[8], although the salt concentration required for dissolution of the globule is less than that predicted by the theory.

However, the effectiveness of salt is suppressed when the size of salt ions is appreciable with respect to polyampholyte chains, or when dense globules has been formed before the addition of salt (Fig.16). The use of the continuous fluid model with enhanced electrical permitivity is shown to

be inaccurate to trace such dynamical processes. In these cases, the salt ions cannot penetrate efficiently into the globules, which makes salt less effective to shield the internal electric field that binds multichain polyampholytes.

ACKNOWLEDGMENTS

The authors, especially M.T., would like to thank Dr.J.-F. Joanny and Dr.S.J. Candau for fruitful discussions and also warm hospitality during his visit to Strasbourg. He is grateful to Dr.T. Hatori for constructive physics discussions, and to Dr.I. Ohmine, Dr.M. Doi, and Dr.K. Yoshikawa, for their interest in the present study. Finally, neat English correction by Dr.J.W. Van Dam is gratefully acknowledged.

REFERENCES

1. C. Tanford, *Physical Chemistry of Macromolecules* (Wiley, New York, 1961).
2. *Protein Folding*, edited L.M. Gierasch and J. King (Amer. Assoc. for Advance. Sci., Washington D.C., 1989).
3. M. Hara, editor, *Polyelectrolytes* (Dekker, New York, 1993).
4. F. Candau and J.F. Joanny, *Encyclopedia of Polymeric Materials, 7*, 5476 (edited by J.C. Salomone, CRC Press, Boca Raton, 1996).
5. M. Mezard, G.Parisi, and M.Virasolo, *Spin Glass Theory and Beyond* (World Sci., Singapore, 1987).
6. J.M. Corpart and F. Candau, *Macromolecules, 26*, 1333 (1993).
7. A. Ohlemacher, F. Candau, J.P. Munch, and S.J. Candau, *J.Polymer Sci., Part B, 34*, 2747 (1996).
8. P.G. Higgs and J.-F. Joanny, *J.Chem.Phys., 94*, 1543 (1990).
9. Y. Kantor, M. Kardar and H. Li, *Phys.Review, E49*, 1383 (1994).
10. A.V. Dobrynin and M. Rubinstein, *J.Phys.II (France), 5*, 677 (1995).
11. R. Everaers, A. Johner, and J.-F. Joanny, *Europhys.Lett., 37*, 275 (1997); *Macromolecules, 30*, 8478 (1997).
12. V.S.Pande, A.Yu.Grosberg, C.Joerg, M.Kardar, and T.Tanaka, *Phys. Rev. Letters, 77*, 3565 (1996).
13. M. Tanaka, A.Yu Grosberg, V.S. Pande, and T. Tanaka, *Phys.Review, E56*, 5798 (1997).
14. T. Soddemann, H. Shiessel and A. Blumen, *Phys.Review, E57*, 2081 (1998).
15. M.Tanaka, A.Yu Grosberg, and T.Tanaka, in *Slow Dynamics in Complex Systems* (edited by M.Tokuyama and I.Oppenheim, AIP Conference Series, 1999).
16. H.Petersen, *J.Chem.Phys., 103*, 3668 (1995).
17. M.Deserno and C.Holm, *How to mesh up Ewald sums (in press)* (1998).
18. C. Kittel and H. Kroemer, *Thermal Physics* (Freeman and Co., San Francisco, 1980).
19. S.M. Kaye and S.L. Marple, *Proc.IEEE, 69*, 1380 (1981).

Table and Caption

T/T_0	$(++/--)$	$(+-/-+)$	$\Delta r^{(++)}$	$\Delta r^{(+-)}$	$N(\Delta r < 1.5a)$
1.00	47%	53%	1.67	1.61	
0.50	44%	56%	1.71	1.49	
0.25	36%	64%	1.46	1.24	
0.125	31%	69%	1.24	0.97	
1.00	44%	56%	–	–	1.15
0.50	41%	59%	–	–	1.19
0.25	40%	60%	–	–	1.83
0.125	43%	57%	–	–	3.40

Table I. Top: The fraction of spatially nearest monomer pairs having equal-sign charges (denoted by $++/--$) and opposite sign charges $(+-/-+)$, and the average distance Δr between such pairs, for randomly co-polymerized multichain polyampholytes (six 32-mers) of overall charge neutrality. Bottom: The fraction of equal /opposite-sign monomers, and the average number of monomers that are located within a sphere of radius $\Delta r < 1.5a$.

FIGURE CAPTIONS

Figure 1. Time evolution of a randomly co-polymerized multichain polyampholyte composed of eight 32-mer chains, for temperature $T/T_0 = 1/2$, at times (a) $\omega_p t = 0$, (b) $\omega_p t = 300$, and (c) $\omega_p t = 600$. The monomers are confined in a spherical domain of radius $R = 21a$. The + and • show the monomers of positive and negative charges, respectively, and the exclusion radius of the monomer is $a_{col} = 0.5a$.

Figure 2. Time history of various quantities for the polyampholyte depicted in Fig. 1: the average elastic energy per monomer W_{spr}, the Coulomb energy per monomer normalized by the base thermal energy Φ_{ES}/T_0, the average bond length of connected monomers $\Delta r^{(c)}$, the system gyration radius including all the monomers $R_{g,sys}$, the average gyration radius of the chains R_{g1}, and the x-component velocity V_x of an individual monomer.

Figure 3. Typical relaxed conformations of eight 32-mer polyampholyte at $\omega_p t = 600$, for temperatures (a) $T/T_0 = 1$, (b) $T/T_0 = 1/4$, and (c) $T/T_0 = 1/8$. A gradual morphological change occurs from the one-phase state with separated chains of (a) to the segregated phase with a collapsed and dense globule of (c) around $T/T_0 \sim 0.3$. The monomers are confined in a spherical domain of radius $R = 21a$, and the exclusion radius of the monomer is $a_{col} = 0.5a$.

Figure 4. Effect of the Coulomb force on structure formation of polyampholytes, as seen in differences between the non-charged polymers and charged polymers of random co-polymerization. The polymers are composed of six 32-mers, and the panels show (a) the system gyration radius $R_{g,sys}$ including all the monomers, (b) the average gyration radius of the chains R_{g1}, and (c) the filling index $N_c^{1/3} R_{g1}/R_{g,sys}$ which indicates chain overlapping, where N_c is the number of chains.

Figure 5. Effect of chain stiffness, for six 32-mer polyampholytes of random co-polymerization. The flexible chains consist of monomers with exclusion radius $a_{col} = 0.5a$, and the stiff ones have $a_{col} = 0.2a$. The panels show (a) the system gyration radius $R_{g,sys}$, (b) the average gyration radius of the chains R_{g1}, and (c) the filling index $N_c^{1/3} R_{g1}/R_{g,sys}$.

Figure 6. (a) Coulomb energy per monomer normalized by the base thermal energy Φ_{ES}/T_0 defined by Eq.(4); (b) deviation of the monomer distances $\delta r_{i,j}$ normalized by the average monomer distance $< r_{i,j} >$, for the flexible and stiff chains in Fig. 5.

Figure 7. Dependence on charge sequences, depicted by three series of runs, in which each of the six 32-mer chains has block size of equal-sign charges of one, two, and then four. The panels show (a) the system gyration radius $R_{g,sys}$, (b) the average gyration radius of the chains R_{g1}, and (c) the filling index $N_c^{1/3} R_{g1}/R_{g,sys}$.

Figure 8. (a) Effect of the domain size (boundary condition) on randomly co-polymerized multichain polyampholytes (six 32-mers), for the case with infinite volume and the case with finite volume of a sphere of radius $R = 21a$. The panels show (a) the system gyration radius $R_{g,sys}$, (b) the average gyration radius of the chains R_{g1}, and (c) the filling index $N_c^{1/3} R_{g1}/R_{g,sys}$. The lower two dots at $T/T_0 < 0.2$ for the infinite volume case of panel (a) are stationary, while the higher two dots increase steadily in time.

Figure 9. Long-time history of the system gyration radius $R_{g,sys}$, for the randomly co-polymerized polyampholytes of Fig.8 with temperatures (a) $T/T_0 = 1/2$, (b) $T/T_0 = 1/4$, and (c) and (d) $T/T_0 = 1/8$. The simulation domain through (a) and (c) is limited by a sphere of radius $R = 21a$, whereas the domain for (d) is infinite.

Figure 10. Time history of the system gyration radius $R_{g,sys}$ of a special run in which the monomer charges of the randomly co-polymerized polyampholyte with temperature $T/T_0 = 1/8$ of Fig. 9(b) are suddenly reset to zero at time $t = 4500\omega_p^{-1}$. The scatter plots show their conformations at (a) $t = 4000\omega_p^{-1}$ and (b) $t = 5000\omega_p^{-1}$.

Figure 11. Dependence on the length (molecular weight) of the chains, for randomly co-polymerized polyampholytes. The number of chains is kept at six, and the panels show (a) the system gyration radius $R_{g,sys}$, (b) the average gyration radius of the chains R_{g1}, and (c) the filling index $N_c^{1/3} R_{g1}/R_{g,sys}$.

Figure 12. Dependence on the number of chains, for randomly co-polymerized polyampholytes. The total number of monomers is kept at 192, and the panels show (a) the system gyration radius $R_{g,sys}$, (b) the average gyration radius of the chains R_{g1}, and (c) the filling index $N_c^{1/3} R_{g1}/R_{g,sys}$.

Figure 13. Frequency spectral analysis with the maximum entropy method for the gyration radius of six 32-mer polyampholyte at (a) high temperature $T/T_0 = 1$ and (b) low temperature $T/T_0 = 1/8$. Each frame corresponds to one specific chain.

Figure 14. Effect of salt addition for the case with 512 salt ions (256 positive and negative free ions), and for the case of enhanced electrical permitivity $\epsilon = 2\epsilon_0$ without salt ions. The polyampholyte is composed of randomly co-polymerized six 32-mers, and the panels show (a) the system gyration radius $R_{g,sys}$, (b) the average gyration radius of the chains R_{g1}, and (c) the filling index $N_c^{1/3} R_{g1}/R_{g,sys}$.

Figure 15. Typical relaxed conformation of randomly co-polymerized polyampholyte (six 32-mers) in salt aqueous solution for the run in Fig. 14 at temperature $T/T_0 = 1/8$: (a) polyampholyte and salt ions; (b) only the polyampholyte. The positive and negative salt ions are marked with $+$ and $\bullet$, respectively. The relaxed conformation of the salt-free polyampholyte for the same temperature is shown in (c).

Figure 16. Effectiveness of added salt. The system gyration radius for the runs in which 512 salt ions are placed in a region excluded by the globule of six 32-mer chains at the intermediate time $t = 1300\omega_p^{-1}$ (denoted by arrows). The temperature is (a) $T/T_0 = 1/4$ and (b) $T/T_0 = 1/8$.

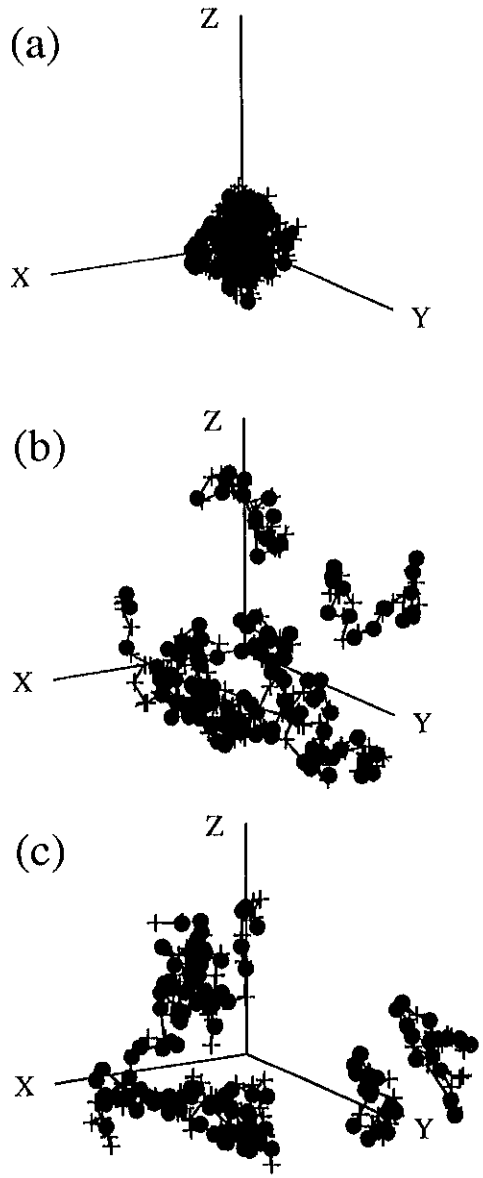

Figure 1

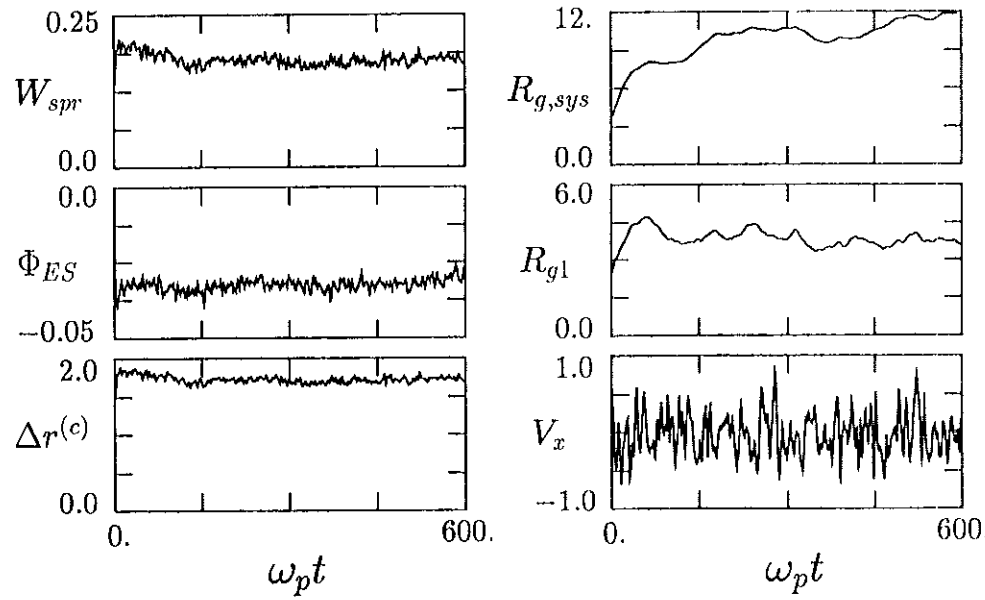

Figure 2

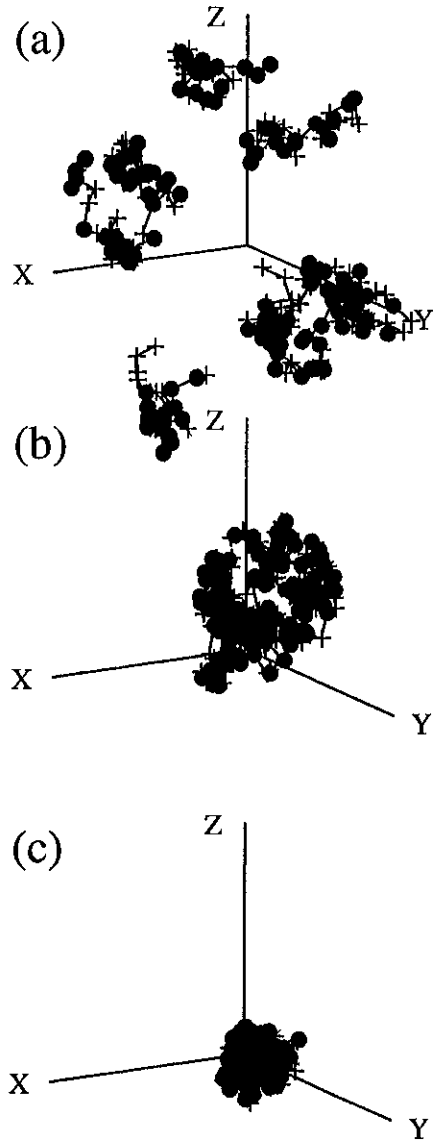

Figure 3

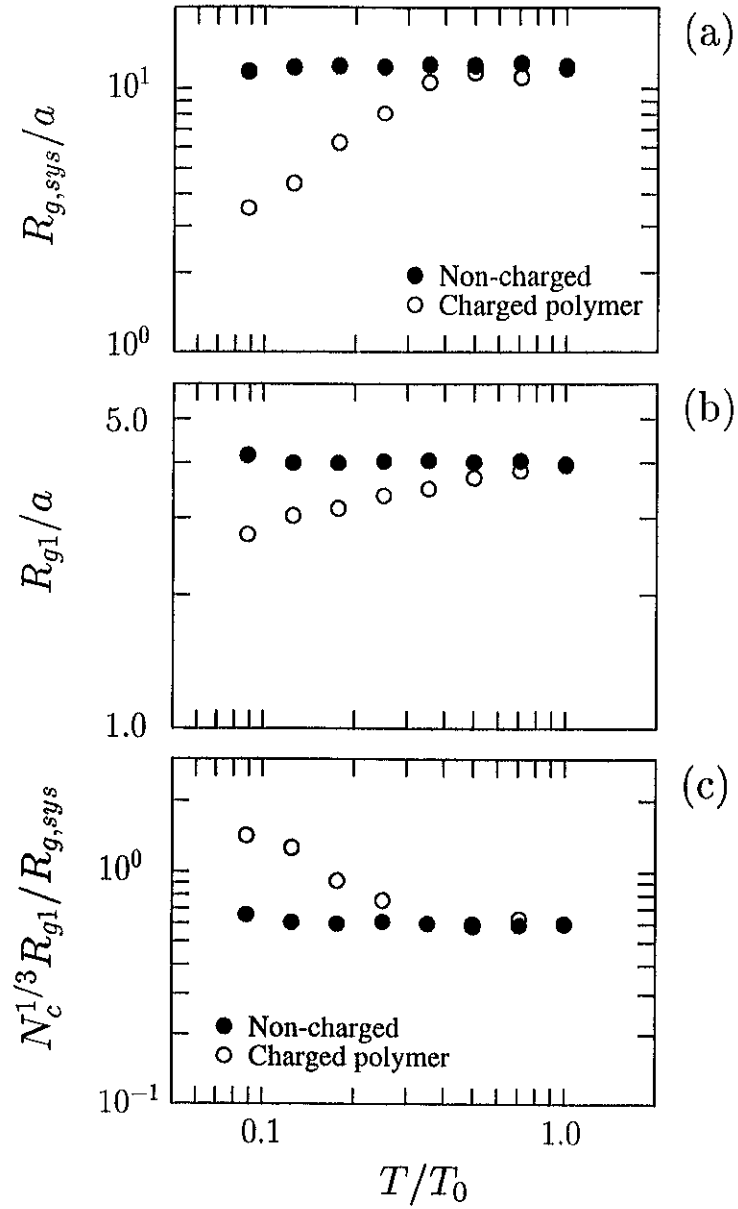

Figure 4

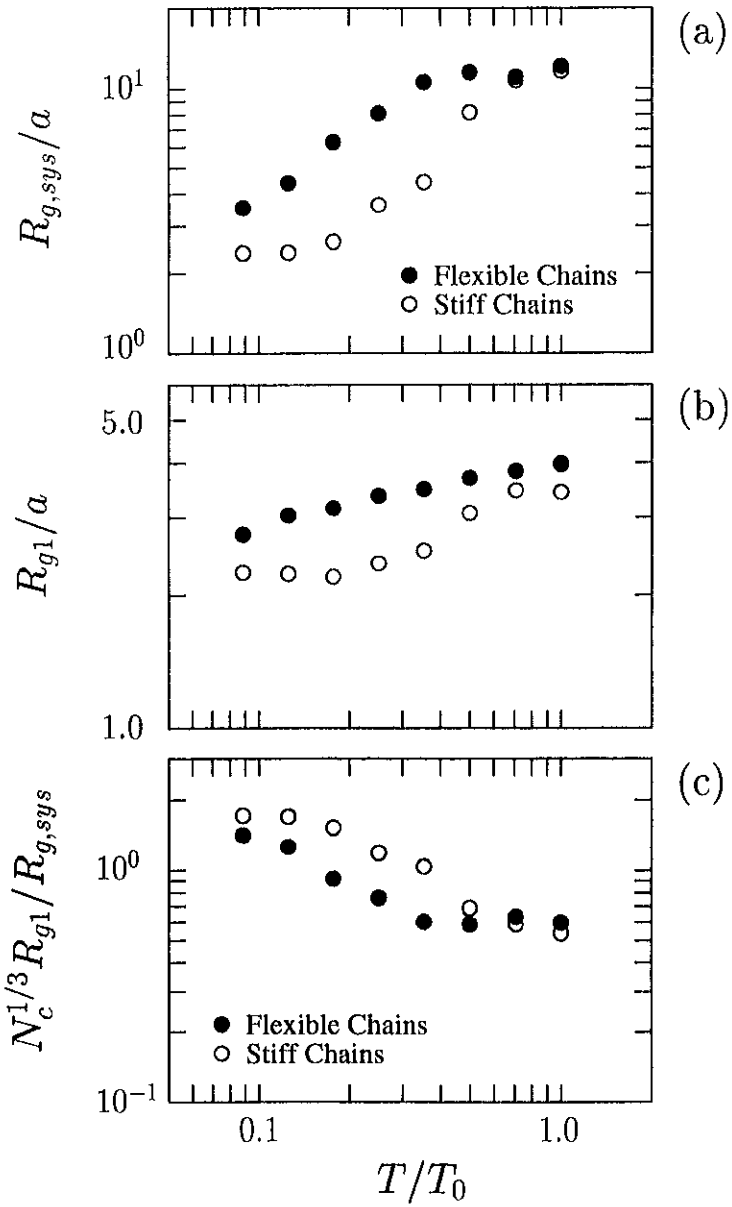

Figure 5

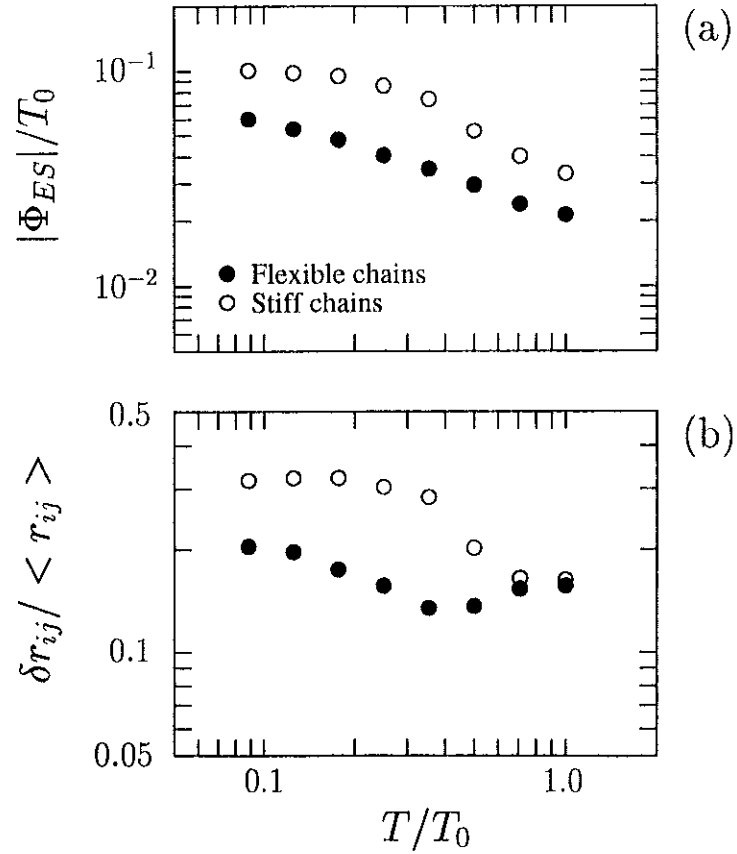

Figure 6

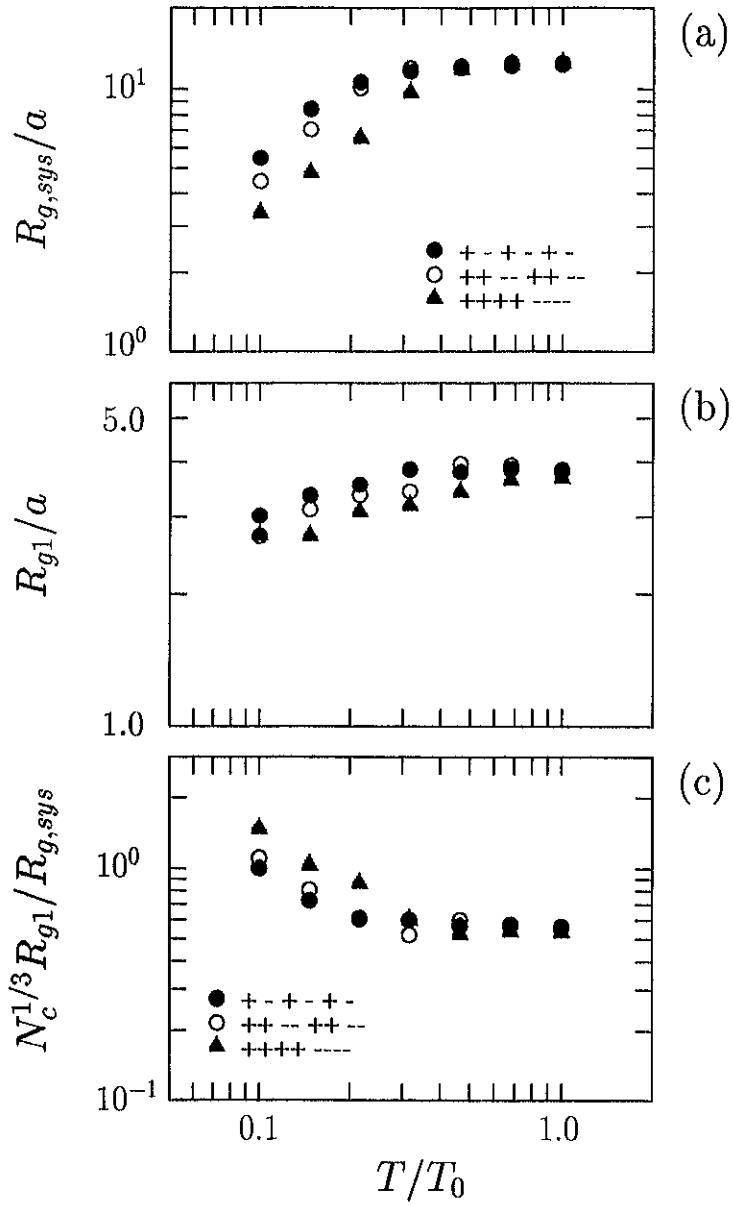

Figure 7

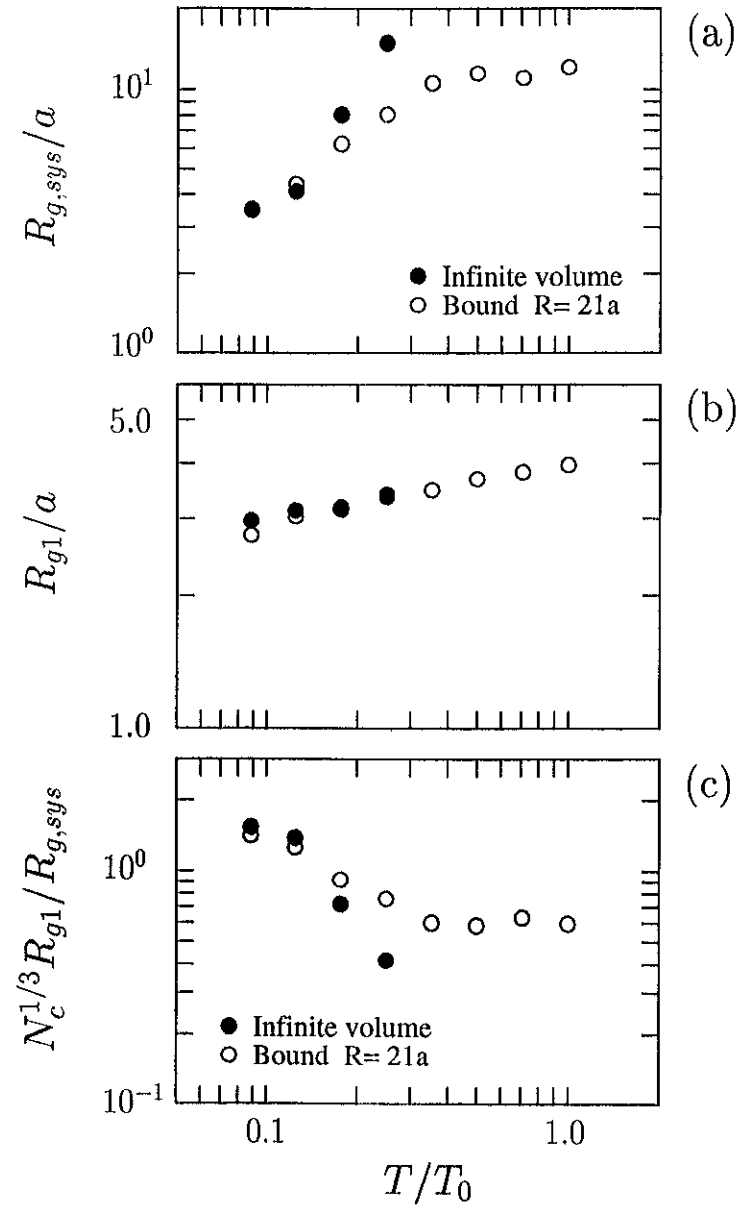

Figure 8

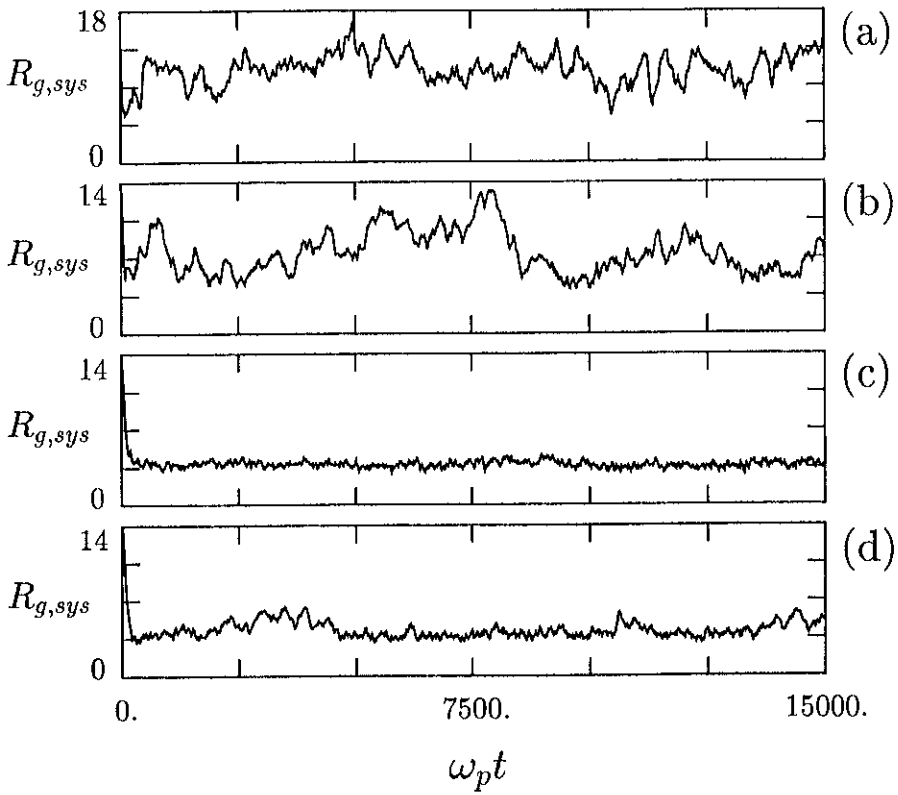

Figure 9

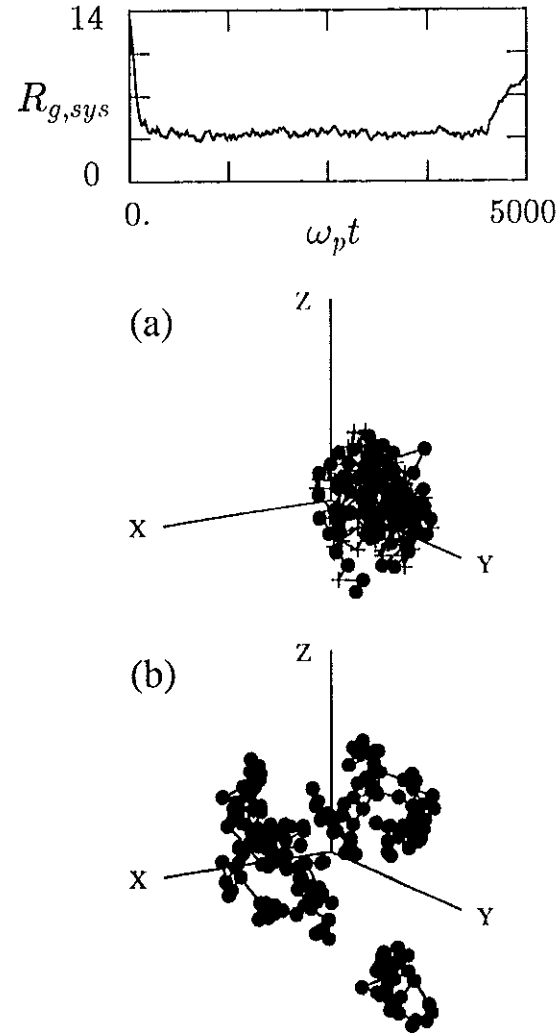

Figure 10

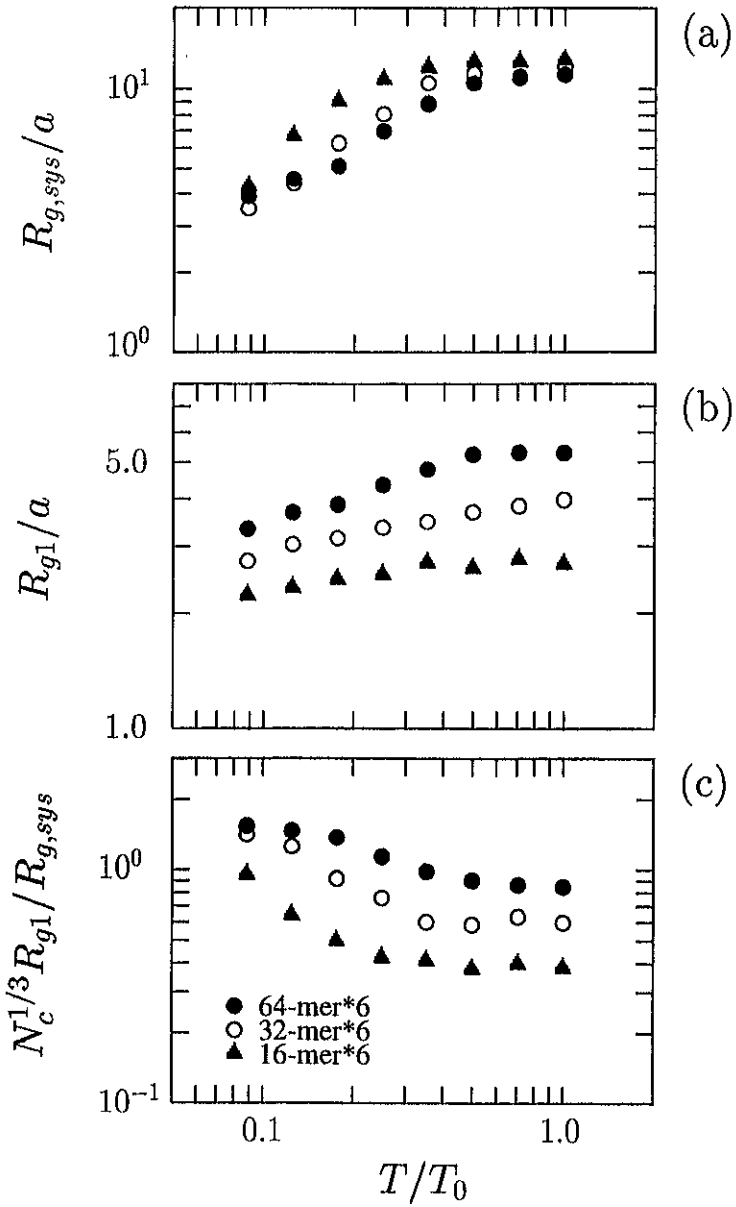

Figure 11

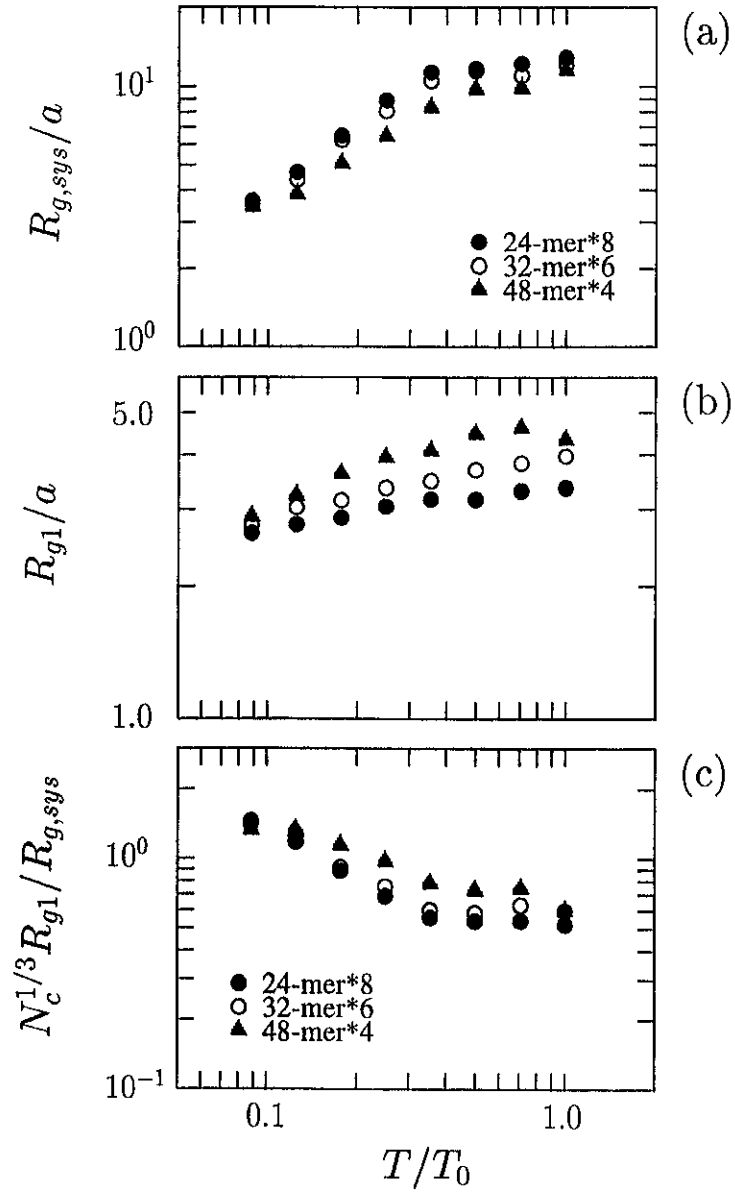

Figure 12

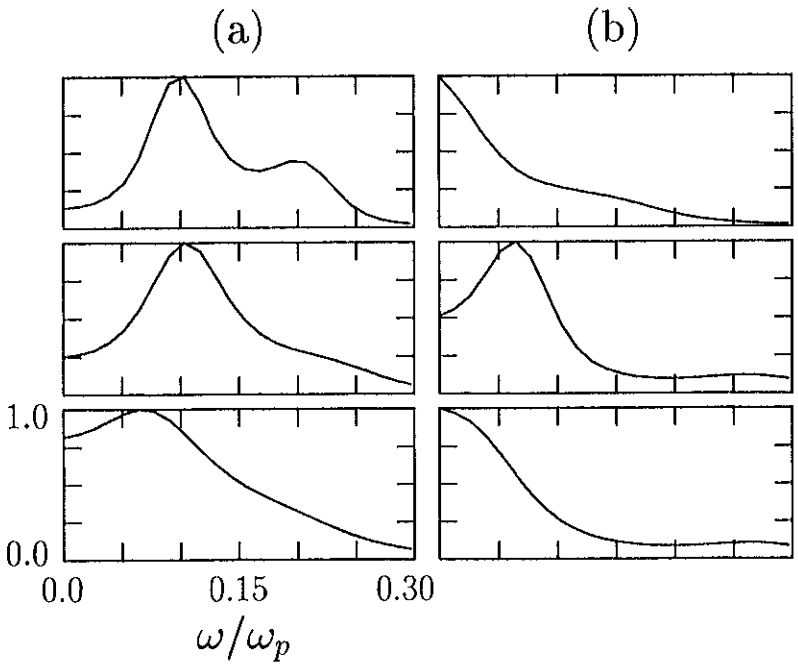

Figure 13

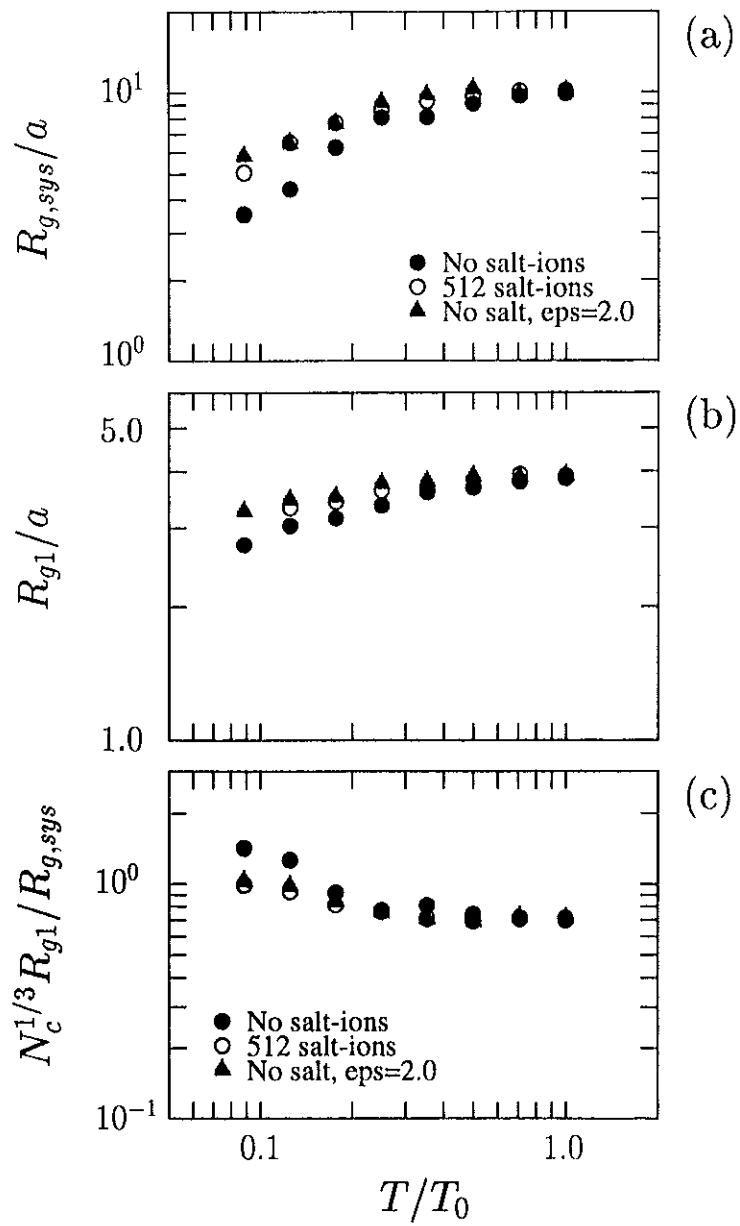

Figure 14

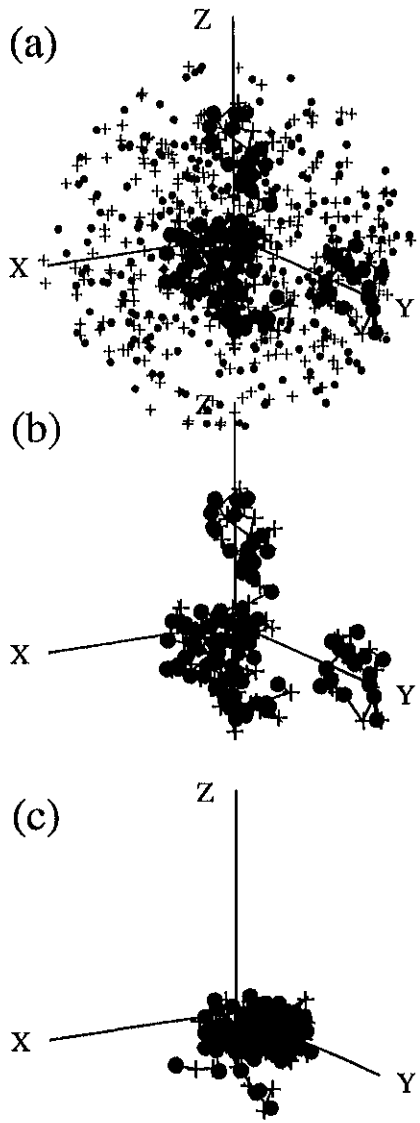

Figure 15

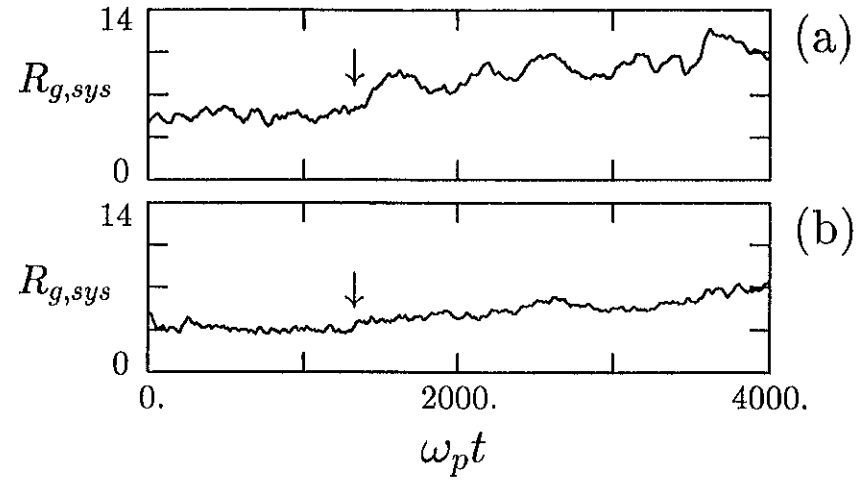

Figure 16

Recent Issues of NIFS Series

NIFS-515 K Akaishi,
On the Solution of the Outgassing Equation for the Pump-down of an Unbaked Vacuum System Oct 1997

NIFS-516 *Papers Presented at the 6th H-mode Workshop (Seeon, Germany)*, Oct 1997

NIFS-517 John L Johnson,
The Quest for Fusion Energy, Oct 1997

NIFS-518 J Chen, N Nakajima and M Okamoto,
Shift-and-Inverse Lanczos Algorithm for Ideal MHD Stability Analysis, Nov 1997

NIFS-519 M. Yokoyama, N Nakajima and M Okamoto,
Nonlinear Incompressible Poloidal Viscosity in L=2 Heliotron and Quasi-Symmetric Stellarators, Nov 1997

NIFS-520 S Kida and H Miura,
Identification and Analysis of Vortical Structures, Nov. 1997

NIFS-521 K Ida, S. Nishimura, T Minami, K Tanaka, S Okamura, M Osakabe, H Idei, S Kubo, C Takahashi and K. Matsuoka,
High Ion Temperature Mode in CHS Heliotron/torsatron Plasmas, Nov. 1997

NIFS-522 M Yokoyama, N Nakajima and M. Okamoto,
Realization and Classification of Symmetric Stellarator Configurations through Plasma Boundary Modulations; Dec 1997

NIFS-523 H Kitauchi,
Topological Structure of Magnetic Flux Lines Generated by Thermal Convection in a Rotating Spherical Shell; Dec. 1997

NIFS-524 T Ohkawa,
Tunneling Electron Trap, Dec 1997

NIFS-525 K. Itoh, S.-I Itoh, M Yagi, A. Fukuyama,
Solitary Radial Electric Field Structure in Tokamak Plasmas, Dec 1997

NIFS-526 Andrey N Lyakhov,
Alfven Instabilities in FRC Plasma, Dec 1997

NIFS-527 J. Uramoto,
Net Current Increment of negative Muonlike Particle Produced by the Electron and Positive Ion Bunch-method; Dec 1997

NIFS-528 Andrey N. Lyakhov,
Comments on Electrostastic Drift Instabilities in Field Reversed Configuraiton; Dec 1997

NIFS-529 J. Uramoto,
Pair Creation of Negative and Positive Pionlike (Muonlike) Particle by Interaction between an Electron Bunch and a Positive Ion Bunch; Dec 1997

NIFS-530 J. Uramoto,
Measuring Method of Decay Time of Negative Muonlike Particle by Beam Collector Applied RF Bias Voltage; Dec 1997

NIFS-531 J. Uramoto,
Confirmation Method for Metal Plate Penetration of Low Energy Negative Pionlike or Muonlike Particle Beam under Positive Ions, Dec. 1997

NIFS 532 J Uramoto,
Pair Creations of Negative and Positive Pionlike (Muonlike) Particle or K Mesonlike (Muonlike) Particle in H2 or D2 Gas Discharge in Magnetic Field, Dec 1997

NIFS-533 S Kawata, C Boonmee, T. Teramoto, L Drska, J Limpouch, R. Liska, M Sinor,
Computer-Assisted Particle-in-Cell Code Development, Dec 1997

NIFS-534 Y Matsukawa, T. Suda, S. Ohnuki and C. Namba,
Microstructure and Mechanical Property of Neutron Irradiated TiNi Shape Memory Alloy; Jan 1998

NIFS-535 A. Fujisawa, H. Iguchi, H. Idei, S. Kubo, K. Matsuoka, S. Okamura, K. Tanaka, T. Minami, S. Ohdachi, S Morita, H Zushi S. Lee, M. Osakabe, R Akiyama, Y. Yoshimura, K. Toi, H. Sanuki, K. Itoh, A. Shimizu, S. Takagi, A. Ejiri, C. Takahashi, M. Kojima, S. Hidekuma, K. Ida, S. Nishimura, N. Inoue, R. Sakamoto, S.-I. Itoh, Y. Hamada, M Fujiwara,
Discovery of Electric Pulsation in a Toroidal Helical Plasma; Jan. 1998

NIFS-536 Lj.R Hadzievski, M.M. Skoric, M. Kono and T. Sato,
Simulation of Weak and Strong Langmuir Collapse Regimes; Jan. 1998

NIFS-537 H. Sugama, W. Horton,
Nonlinear Electromagnetic Gyrokinetic Equation for Plasmas with Large Mean Flows; Feb 1998

NIFS-538 H. Iguchi, T P Crowley, A. Fujisawa, S. Lee, K. Tanaka, T. Minami, S Nishimura, K. Ida, R Akiyama, Y Hamada, H . Idei M. Isobe, M. Kojima, S. Kubo, S. Monta, S. Ohdachi, S. Okamura, M. Osakabe, K. Matsuoka, C. Takahashi and K. Toi,
Space Potential Fluctuations during MHD Activities in the Compact Helical System (CHS), Feb 1998

NIFS-539 Takashi Yabe and Yan Zhang,
Effect of Ambient Gas on Three-Dimensional Breakup in Coronet Formation Process; Feb. 1998

NIFS-540 H. Nakamura, K. Ikeda and S. Yamaguchi,
Transport Coefficients of InSb in a Strong Magnetic Field; Feb. 1998

NIFS-541 J Uramoto,
Development of ν_μ Beam Detector and Large Area ν_μ Beam Source by H_2 Gas Discharge (I), Mar 1998

NIFS-542 J. Uramoto,
Development of $bar\{\nu\}_\mu$ Beam Detector and Large Area $bar\{\nu\}_\mu$ Beam Source by H_2 Gas Discharge (II); Mar. 1998

NIFS-543 J. Uramoto,
Some Problems inside a Mass Analyzer for Pions Extracted from a H_2 Gas Discharge, Mar. 1998

NIFS-544 J. Uramoto,
Simplified ν_μ $bar\{\nu\}_\mu$ Beam Detector and ν_μ $bar\{\nu\}_\mu$ Beam Source by Interaction between an Electron Bunch and a Positive Ion Bunch; Mar 1998

NIFS-545 J. Uramoto,
Various Neutrino Beams Generated by D_2 Gas Discharge; Mar 1998

NIFS-546 R. Kanno, N. Nakajima, T. Hayashi and M. Okamoto,
Computational Study of Three Dunensional Equilibria with the Bootstrap Current; Mar. 1998

NIFS-547 R. Kanno, N. Nakajima and M. Okamoto,
Electron Heat Transport in a Self-Similar Structure of Magnetic Islands; Apr. 1998

NIFS-548 J.E. Rice,
Simulated Impurity Transport in LHD from MIST; May 1998

NIFS-549 M.M. Skoric, T Sato, A.M. Maluckov and M.S. Jovanovic,
On Kinetic Complexity in a Three-Wave Interaction; June 1998

NIFS-550 S. Goto and S. Kida,
Passive Saclar Spectrum in Isotropic Turbulence: Prediction by the Lagrangian Direct-interaction Approximation; June 1998

NIFS-551 T. Kuroda, H. Sugama, R. Kanno, M. Okamoto and W. Horton,
Initial Value Problem of the Toroidal Ion Temperature Gradient Mode ; June 1998

NIFS-552 T. Mutoh, R. Kumazawa, T. Seki, F. Simpo, G. Nomura, T. Ido and T. Watari,

Steady State Tests of High Voltage Ceramic Feedthroughs and Co-Axial Transmission Line of ICRF Heating System for the Large Helical Device ; June 1998

NIFS-553 N Noda K Tsuzuki, A Sagara N Inoue T Muroga,
oronization in Future Devices -Protecting Layer against Tritium and Energetic Neutrals-, July 1998

NIFS-554 S Murakami and H Saleem,
Electromagnetic Effects on Rippling Instability and Tokamak Edge Fluctuations, July 1998

NIFS-555 H Nakamura , K Ikeda and S. Yamaguchi,
Physical Model of Nernst Element, Aug 1998

NIFS-556 H Okumura, S Yamaguchi, H Nakamura, K Ikeda and K Sawada,
Numerical Computation of Thermoelectric and Thermomagnetic Effects, Aug 1998

NIFS-557 Y. Takeiri, M Osakabe, K Tsumori, Y Oka, O Kaneko, E. Asano, T Kawamoto, R. Akiyama and M Tanaka,
Development of a High-Current Hydrogen-Negative Ion Source for LHD-NBI System Aug.1998

NIFS-558 M Tanaka, A Yu Grosberg and T Tanaka,
Molecular Dynamics of Structure Organization of Polyampholytes Sep 1998

NIFS-559 R. Horiuchi, K Nishimura and T Watanabe,
Kinetic Stabilization of Tilt Disruption in Field-Reversed Configurations; Sep 1998
(IAEA-CN-69/THP1/11)

NIFS-560 S Sudo, K Kholopenkov, K. Matsuoka, S Okamura, C Takahashi, R Akiyama, A. Fujisawa, K Ida, H Idei, H Iguchi, M. Isobe S Kado, K. Kondo, S. Kubo, H. Kuramoto, T. Minami, S Morita, S Nishimura, M Osakabe, M. Sasao, B Peterson K Tanaka, K Toi and Y. Yoshimura,
Particle Transport Study with Tracer-Encapsulated Solid Pellet Injection, Oct 1998
(IAEA-CN-69/EXP1/18)

NIFS-561 A Fujisawa, H Iguchi, S. Lee, K Tanaka, T Minami, Y Yoshimura, M. Osakabe, K Matsuoka, S Okamura, H. Idei, S Kubo, S Ohdachi, S Morita, R. Akiyama, K. Toi, H Sanuki, K Itoh, K. Ida, A Shimizu, S. Takagi, C Takahashi, M Kojima, S. Hidekuma, S Nishimura, M Isobe, A. Ejiri, N Inoue, R. Sakamoto, Y. Hamada and M Fujiwara,
Dynamic Behavior Associated with Electric Field Transitions in CHS Heliotron/Torsatron, Oct 1998
(IAEA-CN-69/EX5/1)

NIFS-562 S Yoshikawa,
Next Generation Toroidal Devices, Oct. 1998

NIFS-563 Y Todo and T. Sato,
Kinetic-Magnetohydrodynamic Simulation Study of Fast Ions and Toroidal Alfvén Eigenmodes; Oct 1998
(IAEA-CN-69/THP2/22)

NIFS-564 T Watari, T Shimozuma, Y. Takeiri, R Kumazawa, T. Mutoh, M. Sato, O Kaneko, K Ohkubo, S. Kubo, H Idei, Y Oka, M Osakabe, T. Seki, K Tsumori, Y Yoshimura, R Akiyama, T Kawamoto, S Kobayashi, F Shimpo, Y Takita, E. Asano, S. Itoh, G Nomura, T. Ido, M Hamabe, M. Fujiwara, A Iiyoshi, S Morimoto, T Bigelow and Y P Zhao,
Steady State Heating Technology Development for LHD, Oct. 1998
(IAEA-CN-69/FTP/21)

NIFS-565 A Sagara, K.Y Watanabe, K Yamazaki, O Motojima, M Fujiwara, O Mitarai, S Imagawa, H Yamanishi, H. Chikaraishi, A Kohyama, H. Matsui, T Muroga, T Noda, N. Ohyabu, T Satow, A A Shishkin, S. Tanaka, T Terai and T. Uda,
LHD-Type Compact Helical Reactors, Oct 1998
(IAEA-CN-69/FTP/03(R)

NIFS-566 N Nakajima, J Chen, K. Ichiguchi and M Okamoto,
Global Mode Analysis of Ideal MHD Modes in L=2 Heliotron/Torsatron Systems; Oct 1998
(IAEA-CN-69/THP1/08)

NIFS-567 K Ida, M. Osakabe, K Tanaka, T Minami, S Nishimura, S Okamura, A Fujisawa, Y Yoshimura, S Kubo, R. Akiyama, D S Darrow, H Idei, H Iguchi, M Isobe, S Kado, T Kondo, S Lee K Matsuoka, S Morita, I Nomura, S Ohdachi, M Sasao, A Shimizu, K Tumori, S Takayama, M. Takechi, S Takagi, C Takahashi, K. Toi and T Watari,
Transition from L Mode to High Ion Temperature Mode in CHS Heliotron/Torsatron Plasmas, Oct 1998
(IAEA-CN-69/EX2/2)

NIFS-568 S. Okamura, K Matsuoka, R Akiyama, D S Darrow, A Ejiri, A. Fujisawa, M. Fujiwara, M Goto, K Ida H Idei, H Iguchi, N. Inoue, M. Isobe, K Itoh, S Kado, K. Khlopenkov, T Kondo, S Kubo, A. Lazaros, S Lee, G. Matsunaga, T Minami, S. Morita, S. Murakami, N Nakajima, N Nikai, S. Nishimura, I Nomura, S Ohdachi, K. Ohkuni, M Osakabe, R Pavlichenko, B Peterson, R.

Sakamoto, H. Sanuki, M. Sasao, A. Shimizu, Y Shirai, S. Sudo, S. Takagi, C Takahashi, S. Takayama, M. Takechi, K Tanaka, K. Toi, K. Yamazaki, Y Yoshimura and T. Watari,
Confinement Physics Study in a Small Low-Aspect-Ratio Helical Device CHS. Oct 1998
(IAEA-CN-69/OV4/5)

NIFS-569 M.M. Skonc, T. Sato, A. Maluckov, M.S. Jovanovic,
Micro- and Macro-scale Self-organization in a Dissipative Plasma; Oct. 1998

NIFS-570 T. Hayashi, N. Mizuguchi, T-H. Watanabe, T. Sato and the Complexity Simulation Group,
Nonlinear Simulations of Internal Reconnection Event in Spherical Tokamak; Oct. 1998
(IAEA-CN-69/TH3/3)

NIFS-571 A. Iiyoshi, A. Komori, A. Ejiri, M. Emoto, H. Funaba, M. Goto, K. Ida, H. Idei, S. Inagaki, S. Kado, O. Kaneko, K. Kawahata, S. Kubo, R. Kumazawa, S. Masuzaki, T. Minami, J. Miyazawa, T. Morisaki, S. Morita, S. Murakami, S. Muto, T. Muto, Y. Nagayama, Y. Nakamura, H. Nakanishi, K. Narihara, K. Nishimura, N. Noda, T. Kobuchi, S. Ohdachi, N. Ohyabu, Y. Oka, M. Osakabe, T. Ozaki, B.J. Peterson, A. Sagara, S. Sakakibara, R. Sakamoto, H. Sasao, M. Sasao, K. Sato, M Sato, T Seki, T. Shimozuma, M. Shoji, H. Suzuki, Y Takeiri, K. Tanaka, K. Toi, T. Tokuzawa, K. Tsumori, I. Yamada, H. Yamada, S. Yamaguchi, M Yokoyama, K.Y Watanabe, T. Watari, R. Akiyama, H. Chikaraishi, K. Haba, S Hamaguchi, S Iima, S. Imagawa, N. Inoue, K Iwamoto, S Kitagawa, Y Kubota, J Kodaira, R. Maekawa, T. Mito, T Nagasaka, A. Nishimura, Y. Takita, C Takahashi, K. Takahata, K Yamauchi, H. Tamura, T Tsuzuki, S. Yamada, N. Yanagi, H. Yonezu, Y. Hamada, K. Matsuoka, K Murai, K. Ohkubo, I. Ohtake, M. Okamoto, S. Sato, T. Satow, S. Sudo, S. Tanahashi, K. Yamazaki, M. Fujiwara and O. Motojima,
An Overview of the Large Helical Device Project; Oct. 1998
(IAEA-CN-69/OV1/4)

NIFS-572 M. Fujiwara, H Yamada, A. Ejiri, M. Emoto, H. Funaba, M. Goto, K. Ida, H. Idei, S. Inagaki, S. Kado, O Kaneko, K. Kawahata, A. Komori, S Kubo, R. Kumazawa, S. Masuzaki, T. Minami, J. Miyazawa, T. Morisaki, S. Morita, S. Murakami, S Muto, T. Muto, Y. Nagayama, Y. Nakamura, H. Nakanishi, K. Narihara, K. Nishimura, N. Noda, T. Kobuchi, S. Ohdachi, N Ohyabu, Y. Oka, M. Osakabe, T. Ozaki, B. J. Peterson, A. Sagara, S. Sakakibara, R. Sakamoto, H. Sasao, M. Sasao, K. Sato, M. Sato, T. Seki T Shimozuma, M. Shoji, H. Sazuki, Y. Takeiri, K. Tanaka, K. Toi, T. Tokuzawa, K. Tsumori, I. Yamada, S. Yamaguchi, M. Yokoyama, K.Y Watanabe, T. Watari, R. Akiyama, H. Chikaraishi, K. Haba, S. Hamaguchi, M. Iima, S Imagawa, N. Inoue, K. Iwamoto, S Kitagawa, Y. Kubota, J Kodaira, R. Maekawa, T. Mito, T Nagasaka, A. Nishimura, Y Takita. C. Takahashi, K Takahata, K. Yamauchi, H. Tamura, T. Tsuzuki, S Yamada, N. Yanagi, H Yonezu, Y. Hamada, K. Matsuoka, K. Murai K. Ohkubo, I Ohtake, M Okamoto, S. Sato, T. Satow, S Sudo, S. Tanahashi, K. Yamazaki, O. Motojima and A. Iiyoshi,
Plasma Confinement Studies in LHD: Oct. 1998
(IAEA-CN-69/EX2/3)

NIFS-573 O. Motojima, K. Akaishi, H. Chikaraishi, H. Funaba, S. Hamaguchi, S Imagawa, S. Inagaki, N. Inoue, A. Iwamoto, S. Kitagawa, A. Komori, Y Kubota, R. Maekawa, S. Masuzaki, T. Mito, J. Miyazawa, T. Morisaki, T. Muroga, T. Nagasaka, Y Nakmura, A. Nishimura, K. Nishimura, N. Noda, N. Ohyabu, S. Sagara, S. Sakakibara, R. Sakamoto, S. Satoh, T. Satow, M. Shoji, H. Suzuki, K. Takahata, H. Tamura, K. Watanabe, H. Yamada, S. Yamada, S. Yamaguchi, K. Yamazaki, N. Yanagi, T. Baba, H. Hayashi, M. Iima, T. Inoue, S. Kato, T Kato, T. Kondo, S. Monuchi, H. Ogawa, I. Ohtake, K. Ooba, H. Sekiguchi, N. Suzuki, S. Takami, Y. Taniguchi, T. Tsuzuki, N. Yamamoto, K. Yasui, H. Yonezu, M. Fujiwara and A. Iiyoshi,
Progress Summary of LHD Engineering Design and Construction; Oct. 1998
(IAEA-CN-69/FT2/1)

NIFS-574 K. Toi, M Takechi, S. Takagi, G Matsunaga, M. Isobe, T. Kondo, M. Sasao, D.S. Darrow, K. Ohkuni, S. Ohdachi, R. Akiyama A. Fujisawa, M. Gotoh, H. Idei, K. Ida, H. Iguchi, S. Kado, M. Kojima, S Kubo, S. Lee, K. Matsuoka, T. Minami, S. Morita, N Nikai, S. Nishimura, S. Okamura, M. Osakabe, A. Shimizu, Y. Shirai, C. Takahashi, K. Tanaka, T. Watari and Y. Yoshimura,
Global MHD Modes Excited by Energetic Ions in Heliotron/Torsatron Plasmas; Oct. 1998
(IAEA-CN-69/EXP1/19)

NIFS-575 Y. Hamada, A. Nishizawa, Y. Kawasumi, A. Fujisawa, M. Kojima, K. Narihara, K. Ida, A. Ejiri, S. Ohdachi, K. Kawahata, K. Toi, K. Sato, T. Seki, H Iguchi, K. Adachi, S. Hidekuma, S Hirokura, K. Iwasaki, T. Ido, R Kumazawa, H. Kuramoto T. Minami, I.. Nomura, M. Sasao, K.N. Sato, T. Tsuzuki, I. Yamada and T Watari,
Potential Turbulence in Tokamak Plasmas; Oct. 1998
(IAEA-CN-69/EXP2/14)

NIFS-576 S. Murakami, U. Gasparino, H. Idei, S. Kubo, H. Maassberg, N. Marushchenko, N. Nakajima, M. Romé and M. Okamoto,
5D Simulation Study of Suprathermal Electron Transport in Non-Axisymmetric Plasmas; Oct. 1998
(IAEA-CN-69/THP1/01)

NIFS-577 S. Fujiwara and T. Sato,
Molecular Dynamics Simulation of Structure Formation of Short Chain Molecules; Nov 1998

NIFS-578 T. Yamagishi,
Eigenfunctions for Vlasov Equation in Multi-species Plasmas Nov. 1998

NIFS-579 M. Tanaka, A. Yu Grosberg and T. Tanaka,
Molecular Dynamics of Strongly-Coupled Multichain Coulomb Polymers in Pure and Salt Aqueous Solutions; Nov. 1998